Available online at www.sciencedirect.com
ScienceDirect
Comput. Methods Appl. Mech. Engrg. 325 (2017) 155–174
Computer methods in applied mechanics and engineering
www.elsevier.com/locate/cma

# A stress/displacement Virtual Element method for plane elasticity problems

E. Artioli[a,*], S. de Miranda[b], C. Lovadina[c,d], L. Patruno[b]

[a] *Department of Civil Engineering and Computer Science, University of Rome Tor Vergata, Via del Politecnico 1, 00133 Rome, Italy*
[b] *DICAM, University of Bologna, Viale Risorgimento 2, 40136 Bologna, Italy*
[c] *Dipartimento di Matematica, Università di Milano, Via Saldini 50, 20133 Milano, Italy*
[d] *IMATI del CNR, Via Ferrata 1, 27100 Pavia, Italy*

Received 5 February 2017; received in revised form 21 May 2017; accepted 29 June 2017
Available online 13 July 2017

**Abstract**

The numerical approximation of 2D elasticity problems is considered, in the framework of the small strain theory and in connection with the mixed Hellinger–Reissner variational formulation. A low-order Virtual Element Method (VEM) with a priori symmetric stresses is proposed. Several numerical tests are provided, along with a rigorous stability and convergence analysis.


*Keywords:* Virtual element method; Hellinger–Reissner; Symmetric stress; Elasticity; Low order method

## 1. Introduction

The Virtual Element Method (VEM) is a new technology for the approximation of partial differential equation problems. VEM was born in 2012, see [1], as an evolution of modern mimetic schemes (see for instance [2–4]), which shares the same variational background of the Finite Element Method (FEM). The initial motivation of VEM is the need to construct an accurate *conforming* Galerkin scheme with the capability to deal with highly general polygonal/polyhedral meshes, including "hanging vertexes" and non-convex shapes. The virtual element method reaches this goal by *abandoning the local polynomial approximation concept*, and uses, instead, approximating functions which are solutions to suitable local partial differential equations (of course, connected with the original problem to solve). Therefore, in general, the discrete functions are not known pointwise, but a limited information of them is at disposal. The key point is that the available information are indeed sufficient to implement the stiffness matrix and the right-hand side. We remark that VEM is not the only available technology for dealing with polytopal meshes: a brief representative sample of the increasing list of technologies that make use of polygonal/polyhedral

* Corresponding author.
*E-mail addresses:* artioli@ing.uniroma2.it (E. Artioli), stefano.demiranda@unibo.it (S. de Miranda), carlo.lovadina@unimi.it (C. Lovadina), luca.patruno@unibo.it (L. Patruno).

http://dx.doi.org/10.1016/j.cma.2017.06.036
0045-7825/

meshes can be found in [4–22]. We here recall, in particular, the polygonal finite elements and the mimetic discretization schemes. However, VEM is experiencing a growing interest towards Structural Mechanics problems, also in the engineering community. We here cite the recent works [23–29] and [30,31], for instance.

In the present paper we apply the VEM concept to two-dimensional elasticity problems in the framework of small displacements and small deformations. More precisely, we consider the (mixed) Hellinger–Reissner functional (see, for instance, [32,33]) as the starting point of the discretization procedure. Thus, the numerical scheme approximates both the stress and displacement fields.

It is well-known that in the Finite Element practice, designing a stable and accurate conforming element for the Hellinger–Reissner functional, is not at all a trivial task. Essentially, one is led either to consider quite cumbersome schemes, or to relax the symmetry of the Cauchy stress field, or to employ composite elements (a discussion about this issue can be found in [32], for instance). We here exploit the flexibility of the VEM approach to propose and study *a low-order scheme, with a priori symmetric Cauchy stresses, that can be used for general polygons, from triangular shapes on*. Furthermore, the method is robust with respect to the compressibility parameter, and therefore can be used for nearly incompressible situations. Our scheme approximates the stress field by using traction degrees of freedom (three per each edge), while the displacement field inside each polygon is essentially a rigid body motion. The VEM concept is then applied primarily for the stress field. We also remark that the construction of the discrete stress field is somehow similar to the construction of the discrete velocity field used for the Stokes problem in [34]. Instead, the displacement field is modelled with polynomial functions, in accordance with the classical Finite Element procedure.

An outline of the paper is as follows. In Section 2 we briefly introduce the Hellinger–Reissner variational formulation of the elasticity problem. Section 3 concerns with the discrete problem: all the bilinear and linear forms are introduced and detailed. Numerical experiments are reported in Section 4, where suitable error measures are considered. These numerical tests are supported by the stability and convergence analysis developed in Section 5. Finally, Section 6 draws some conclusions, including possible future extensions of the present study.

Throughout the paper, given two quantities $a$ and $b$, we use the notation $a \lesssim b$ to mean: there exists a constant $C$, independent of the mesh-size, such that $a \leq C\, b$. Moreover, we use standard notations for Sobolev spaces, norms and semi-norms (cf. [35], for example).

## 2. The elasticity problem in mixed form

In this section we briefly present the elasticity problem as it stems from the Hellinger–Reissner principle. More details can be found in [32,33]. We thus consider the following problem.

$$\begin{cases} \text{Find } (\boldsymbol{\sigma}, \mathbf{u}) \text{ such that} \\ -\mathbf{div}\,\boldsymbol{\sigma} = \mathbf{f} \qquad \text{in } \Omega \\ \boldsymbol{\sigma} = \mathbb{C}\boldsymbol{\varepsilon}(\mathbf{u}) \qquad \text{in } \Omega \\ \mathbf{u}_{|\partial\Omega} = \mathbf{0}. \end{cases} \tag{1}$$

Defining $(\cdot,\cdot)$ as the scalar product in $L^2$, $\mathbb{D} := \mathbb{C}^{-1}$, and $a(\boldsymbol{\sigma}, \boldsymbol{\tau}) := (\mathbb{D}\boldsymbol{\sigma}, \boldsymbol{\tau})$, a mixed variational formulation of the problem reads:

$$\begin{cases} \text{Find } (\boldsymbol{\sigma}, \mathbf{u}) \in \Sigma \times U \text{ such that} \\ a(\boldsymbol{\sigma}, \boldsymbol{\tau}) + (\mathbf{div}\,\boldsymbol{\tau}, \mathbf{u}) = 0 \quad \forall \boldsymbol{\tau} \in \Sigma \\ (\mathbf{div}\,\boldsymbol{\sigma}, \mathbf{v}) = -(\mathbf{f}, \mathbf{v}) \quad \forall \mathbf{v} \in U \end{cases} \tag{2}$$

where $\Omega \subset \mathbb{R}^2$ is a polygonal domain, $U = L^2(\Omega)^2$, the loading $\mathbf{f} \in L^2(\Omega)^2$ and

$$\Sigma = \{\boldsymbol{\tau} \in H(\mathbf{div}\,; \Omega) \ : \ \boldsymbol{\tau} \text{ is symmetric}\}\,.$$

We recall that **div** is the vector-valued divergence operator, acting on a second order tensor field. Thus, $\mathbf{div}\,\boldsymbol{\tau}$ is, in Cartesian components: $\frac{\partial \tau_{ij}}{\partial x_j}$ (Einstein's summation convention is here adopted). Moreover, as usual, $H(\mathbf{div}\,; \Omega)$ denotes the space of tensor in $L^2(\Omega)^{2\times 2}$, whose divergence is in $L^2(\Omega)^2$.

The elasticity fourth-order symmetric tensor $\mathbb{D} = \mathbb{C}^{-1}$ is assumed to be uniformly bounded and positive-definite. It is well known that Problem (2) is well-posed (see [32], for instance). In particular, it holds:

$$\|\boldsymbol{\sigma}\|_{\Sigma} + \|\mathbf{u}\|_{U} \leq C \|\mathbf{f}\|_0, \tag{3}$$

where $C$ is a constant depending on $\Omega$ and on the material tensor $\mathbb{C}$.

Note also that the bilinear form $a(\cdot,\cdot)$ in (2) can obviously be split as

$$a(\boldsymbol{\sigma},\boldsymbol{\tau}) = \sum_{E\in\mathcal{T}_h} a_E(\boldsymbol{\sigma},\boldsymbol{\tau}) \quad \text{with} \quad a_E(\boldsymbol{\sigma},\boldsymbol{\tau}) := \int_E \mathbb{D}\boldsymbol{\sigma} : \boldsymbol{\tau} \tag{4}$$

for all $\boldsymbol{\sigma},\boldsymbol{\tau} \in \Sigma$. Above, $\mathcal{T}_h$ is a polygonal mesh of meshsize $h$.

Similarly, it holds

$$(\mathbf{div}\,\boldsymbol{\tau},\mathbf{v}) = \sum_{E\in\mathcal{T}_h} (\mathbf{div}\,\boldsymbol{\tau},\mathbf{v})_E \quad \text{with} \quad (\mathbf{div}\,\boldsymbol{\tau},\mathbf{v})_E := \int_E \mathbf{div}\,\boldsymbol{\tau}\cdot\mathbf{v}, \tag{5}$$

for all $(\boldsymbol{\tau},\mathbf{v}) \in \Sigma \times U$.

**Remark 1.** As discussed in [32], estimate (3) does not break down for nearly incompressible materials. More precisely, considering the constitutive law:

$$\mathbb{C}\boldsymbol{\varepsilon} = 2\mu\boldsymbol{\varepsilon} + \lambda \mathrm{tr}(\boldsymbol{\varepsilon}) Id \qquad \forall \text{ symmetric tensor } \boldsymbol{\varepsilon}, \tag{6}$$

with $\lambda, \mu > 0$ the Lamé's parameters and $\mathrm{tr}(\cdot)$ the trace operator, the constant $C$ in (3) can be chosen independent of $\lambda$. The key point is that it is sufficient to check the $\Sigma$-coercivity of the bilinear form $a(\cdot,\cdot)$ in (2) for the subspace:

$$K = \{\boldsymbol{\tau} \in \Sigma \,:\, (\mathbf{div}\,\boldsymbol{\tau},\mathbf{v}) = 0 \quad \forall \mathbf{v} \in U\}. \tag{7}$$

In fact, there exists a positive constant $\alpha$ such that (see [32]):

$$a(\boldsymbol{\tau},\boldsymbol{\tau}) \geq \alpha \|\boldsymbol{\tau}\|^2_\Sigma \qquad \forall \boldsymbol{\tau} \in K, \tag{8}$$

with $\alpha$ independent of $\lambda$.

## 3. The virtual element method

We outline the Virtual Element discretization of Problem (2). Let $\{\mathcal{T}_h\}_h$ be a sequence of decompositions of $\Omega$ into general polygonal elements $E$ with

$$h_E := \mathrm{diameter}(E), \qquad h := \sup_{E\in\mathcal{T}_h} h_E.$$

In what follows, $|E|$ and $|e| = h_e$ will denote the area of $E$ and the length of the side $e \in \partial E$, respectively.

We suppose that for all $h$, each element $E$ in $\mathcal{T}_h$ fulfils the following assumptions:

- (**A1**) $E$ is star-shaped with respect to a ball of radius $\geq \gamma\, h_E$,
- (**A2**) the distance between any two vertexes of $E$ is $\geq c\, h_E$,

where $\gamma$ and $c$ are positive constants. We remark that the hypotheses above, though not too restrictive in many practical cases, can be further relaxed, as noted in [1].

Our Virtual Element method is based on the following procedure.

1. We first approximate the tensor $\mathbb{D}$ with $\bar{\mathbb{D}}$, a suitable piecewise constant with respect to the underlying mesh $\mathcal{T}_h$ (e.g. we could take the local mean value of $\mathbb{D}$, component-wise). Accordingly, we consider the problem:

$$\begin{cases} \text{Find } (\bar{\boldsymbol{\sigma}},\bar{\mathbf{u}}) \text{ such that} \\ -\mathbf{div}\,\bar{\boldsymbol{\sigma}} = \mathbf{f} \qquad \text{in } \Omega \\ \bar{\mathbb{D}}\bar{\boldsymbol{\sigma}} = \boldsymbol{\varepsilon}(\bar{\mathbf{u}}) \qquad \text{in } \Omega \\ \bar{\mathbf{u}}_{|\partial\Omega} = \mathbf{0}. \end{cases} \tag{9}$$

2. We then approximate Problem (9) by an appropriate Virtual Element scheme which returns a discrete solution $(\boldsymbol{\sigma}_h,\mathbf{u}_h)$ satisfying

$$\|\bar{\boldsymbol{\sigma}} - \boldsymbol{\sigma}_h\|_\Sigma + \|\bar{\mathbf{u}} - \mathbf{u}_h\|_0 \lesssim h. \tag{10}$$

We now show that, for smooth tensors $\mathbb{D}$, the discrete solution $(\boldsymbol{\sigma}_h, \mathbf{u}_h)$ is also a first order approximation of $(\boldsymbol{\sigma}, \mathbf{u})$, solution to the original Problem (1). More precisely, we assume that:

$$\text{Each component } \mathbb{D}_{ijkl} \text{ of } \mathbb{D} \text{ is such that } \mathbb{D}_{ijkl|E} \in H^1(E) \text{ for every } E \in \mathcal{T}_h. \tag{11}$$

We have the following result.

**Proposition 3.1.** *Let* $(\boldsymbol{\sigma}, \mathbf{u})$ *solve* (1)*, and let* $(\bar{\boldsymbol{\sigma}}, \bar{\mathbf{u}})$ *solve* (9)*. Under assumption* (11)*, it holds*

$$\|\boldsymbol{\sigma} - \bar{\boldsymbol{\sigma}}\|_{\Sigma} + \|\mathbf{u} - \bar{\mathbf{u}}\|_1 \lesssim \left( \sum_{E \in \mathcal{T}_h} h_E^2 |\mathbb{D}|_{1,E}^2 \right)^{1/2} \|\mathbf{f}\|_0. \tag{12}$$

*In addition, if* $(\boldsymbol{\sigma}_h, \mathbf{u}_h)$ *fulfils* (10)*, then*

$$\|\boldsymbol{\sigma} - \boldsymbol{\sigma}_h\|_{\Sigma} + \|\mathbf{u} - \mathbf{u}_h\|_0 \lesssim h. \tag{13}$$

**Proof.** Due to the uniform boundedness and positive-definiteness of $\mathbb{D}$, together with the Korn's inequality, it follows that

$$\|\boldsymbol{\sigma} - \bar{\boldsymbol{\sigma}}\|_0^2 + \|\mathbf{u} - \bar{\mathbf{u}}\|_1^2 \lesssim \int_{\Omega} \mathbb{D}(\boldsymbol{\sigma} - \bar{\boldsymbol{\sigma}}) : (\boldsymbol{\sigma} - \bar{\boldsymbol{\sigma}}) + \int_{\Omega} \mathbb{C}(\boldsymbol{\varepsilon}(\mathbf{u} - \bar{\mathbf{u}})) : (\boldsymbol{\varepsilon}(\mathbf{u} - \bar{\mathbf{u}})). \tag{14}$$

By the Hyper-Circle Theorem of Prager and Synge (see [36]), it holds

$$\int_{\Omega} \mathbb{D}(\boldsymbol{\sigma} - \bar{\boldsymbol{\sigma}}) : (\boldsymbol{\sigma} - \bar{\boldsymbol{\sigma}}) + \int_{\Omega} \mathbb{C}(\boldsymbol{\varepsilon}(\mathbf{u} - \bar{\mathbf{u}})) : (\boldsymbol{\varepsilon}(\mathbf{u} - \bar{\mathbf{u}})) = \int_{\Omega} \mathbb{D}(\bar{\boldsymbol{\sigma}} - \mathbb{C}\boldsymbol{\varepsilon}(\bar{\mathbf{u}})) : (\bar{\boldsymbol{\sigma}} - \mathbb{C}\boldsymbol{\varepsilon}(\bar{\mathbf{u}})). \tag{15}$$

We now notice that $\mathbb{D}(\bar{\boldsymbol{\sigma}} - \mathbb{C}\boldsymbol{\varepsilon}(\bar{\mathbf{u}})) = \mathbb{D}(\bar{\boldsymbol{\sigma}} - \mathbb{C}\bar{\mathbb{D}}\bar{\boldsymbol{\sigma}}) = (\mathbb{D} - \bar{\mathbb{D}})\bar{\boldsymbol{\sigma}}$ (see (9)). Hence, using the uniform boundedness of $\mathbb{C}$ and standard approximation results, we infer

$$\begin{aligned} \int_{\Omega} \mathbb{D}(\bar{\boldsymbol{\sigma}} - \mathbb{C}\boldsymbol{\varepsilon}(\bar{\mathbf{u}})) : (\bar{\boldsymbol{\sigma}} - \mathbb{C}\boldsymbol{\varepsilon}(\bar{\mathbf{u}})) = \int_{\Omega} (\mathbb{D} - \bar{\mathbb{D}})\bar{\boldsymbol{\sigma}} \, : \mathbb{C}((\mathbb{D} - \bar{\mathbb{D}})\bar{\boldsymbol{\sigma}}) &\lesssim \|(\mathbb{D} - \bar{\mathbb{D}})\bar{\boldsymbol{\sigma}}\|_0^2 \\ &\lesssim \left( \sum_{E \in \mathcal{T}_h} h_E^2 |\mathbb{D}|_{1,E}^2 \right) \|\bar{\boldsymbol{\sigma}}\|_0^2. \end{aligned} \tag{16}$$

Furthermore, we notice that $\mathbf{div}(\boldsymbol{\sigma} - \bar{\boldsymbol{\sigma}}) = \mathbf{0}$. Therefore, combining (14)–(16), and using the stability bound $\|\bar{\boldsymbol{\sigma}}\|_0 \lesssim \|\mathbf{f}\|_0$ we obtain

$$\|\boldsymbol{\sigma} - \bar{\boldsymbol{\sigma}}\|_{\Sigma}^2 + \|\mathbf{u} - \bar{\mathbf{u}}\|_1^2 \lesssim \left( \sum_{E \in \mathcal{T}_h} h_E^2 |\mathbb{D}|_{1,E}^2 \right) \|\mathbf{f}\|_0^2, \tag{17}$$

i.e. estimate (12). From (17) we immediately get

$$\|\boldsymbol{\sigma} - \bar{\boldsymbol{\sigma}}\|_{\Sigma} + \|\mathbf{u} - \bar{\mathbf{u}}\|_0 \lesssim h \, \|\mathbf{f}\|_0, \tag{18}$$

and estimate (13) now follows using (10) and the triangle inequality. □

**Remark 2.** Proposition 3.1 shows that one may assume that $\mathbb{D}$ is piecewise constant *ab initio*: if an error bound like (10) holds true, then the convergence estimate (13) is valid for $\mathbb{D}$ satisfying assumption (11) as well. This is the approach we follow in the sequel of the paper.

**Remark 3.** Proposition 3.1 allows for elastic coefficients which might be discontinuous (for instance, the case of a body made of two different homogeneous materials). However, possible discontinuities should be aligned with the mesh. This is encoded into hypothesis (11).

### 3.1. The local spaces

Given a polygon $E \in \mathcal{T}_h$ with $n_E$ edges, we first introduce the space of local infinitesimal rigid body motions:

$$RM(E) = \left\{ \mathbf{r}(\mathbf{x}) = \mathbf{a} + b(\mathbf{x} - \mathbf{x}_C)^\perp \quad \mathbf{a} \in \mathbb{R}^2,\ b \in \mathbb{R} \right\}. \tag{19}$$

Here above, given $\mathbf{c} = (c_1, c_2)^T \in \mathbb{R}^2$, $\mathbf{c}^\perp$ is the counterclock-wise rotated vector $\mathbf{c}^\perp = (c_2, -c_1)^T$, and $\mathbf{x}_C$ is the barycentre of $E$. For each edge $e$ of $\partial E$, we introduce the space

$$R(e) = \left\{ \mathbf{t}(s) = \mathbf{c} + d\, s\, \mathbf{n} \quad \mathbf{c} \in \mathbb{R}^2,\ d \in \mathbb{R},\ s \in [-1/2, 1/2] \right\}. \tag{20}$$

Here above, $s$ is a local linear coordinate on $e$, such that $s = 0$ corresponds to the edge midpoint. Furthermore, $\mathbf{n}$ is the outward normal to the edge $e$. Hence, $R(e)$ consists of vectorial functions which have the edge tangential component constant, and the edge normal component linear along the edge. Our local approximation space for the stress field is then defined by

$$\begin{aligned} \Sigma_h(E) = \Big\{ & \boldsymbol{\tau}_h \in H(\mathbf{div}; E) \ :\ \exists \mathbf{w}^* \in H^1(E)^2 \text{ such that } \boldsymbol{\tau}_h = \mathbb{C}\boldsymbol{\varepsilon}(\mathbf{w}^*); \\ & (\boldsymbol{\tau}_h\, \mathbf{n})_{|e} \in R(e) \quad \forall e \in \partial E; \quad \mathbf{div}\, \boldsymbol{\tau}_h \in RM(E) \Big\}. \end{aligned} \tag{21}$$

**Remark 4.** Alternatively, the space (21) can be defined as follows.

$$\begin{aligned} \Sigma_h(E) = \Big\{ & \boldsymbol{\tau}_h \in H(\mathbf{div}; E) \ :\ \boldsymbol{\tau}_h = \boldsymbol{\tau}_h^T; \quad \mathrm{curl}\, \mathbf{curl}(\mathbb{D}\boldsymbol{\tau}_h) = 0; \\ & (\boldsymbol{\tau}_h\, \mathbf{n})_{|e} \in R(e) \quad \forall e \in \partial E; \quad \mathbf{div}\, \boldsymbol{\tau}_h \in RM(E) \Big\}. \end{aligned} \tag{22}$$

Here above, the equation $\mathrm{curl}\, \mathbf{curl}(\mathbb{D}\boldsymbol{\tau}_h) = 0$ is to be intended in the distribution sense.

We remark that, once $(\boldsymbol{\tau}_h\, \mathbf{n})_{|e} = \mathbf{c}_e + d_e s\, \mathbf{n}$ is given for all $e \in \partial E$, cf. (20), the quantity $\mathbf{div}\, \boldsymbol{\tau}_h \in RM(E)$ is determined. Indeed, denoting with $\boldsymbol{\varphi} : \partial E \to \mathbb{R}^2$ the function such that $\boldsymbol{\varphi}_{|e} := \mathbf{c}_e + d_e s\, \mathbf{n}$, the obvious compatibility condition

$$\int_E \mathbf{div}\, \boldsymbol{\tau}_h \cdot \mathbf{r} = \int_{\partial E} \boldsymbol{\varphi} \cdot \mathbf{r} \qquad \forall \mathbf{r} \in RM(E), \tag{23}$$

allows to compute $\mathbf{div}\, \boldsymbol{\tau}_h$ using the $\mathbf{c}_e$'s and the $d_e$'s. More precisely, setting (cf. (19))

$$\mathbf{div}\, \boldsymbol{\tau}_h = \boldsymbol{\alpha}_E + \beta_E (\mathbf{x} - \mathbf{x}_C)^\perp, \tag{24}$$

from (23) we infer

$$\begin{cases} \boldsymbol{\alpha}_E = \dfrac{1}{|E|} \displaystyle\int_{\partial E} \boldsymbol{\varphi} = \frac{1}{|E|} \sum_{e \in \partial E} \int_e \mathbf{c}_e \\ \beta_E = \dfrac{1}{\int_E |\mathbf{x} - \mathbf{x}_C|^2} \displaystyle\int_{\partial E} \boldsymbol{\varphi} \cdot (\mathbf{x} - \mathbf{x}_C)^\perp = \frac{1}{\int_E |\mathbf{x} - \mathbf{x}_C|^2} \sum_{e \in \partial E} \int_e (\mathbf{c}_e + d_e s\, \mathbf{n}) \cdot (\mathbf{x} - \mathbf{x}_C)^\perp. \end{cases} \tag{25}$$

The local approximation space for the displacement field is simply defined by, see (19):

$$U_h(E) = \left\{ \mathbf{v}_h \in L^2(E)^2 \ :\ \mathbf{v}_h \in RM(E) \right\}. \tag{26}$$

We notice that $\dim(\Sigma_h(E)) = 3\, n_E$, while $\dim(U_h(E)) = 3$.

### 3.2. The local bilinear forms

Given $E \in \mathcal{T}_h$, we first notice that, for every $\boldsymbol{\tau}_h \in \Sigma_h(E)$ and $\mathbf{v}_h \in U_h(E)$, the term

$$\int_E \mathbf{div}\, \boldsymbol{\tau}_h \cdot \mathbf{v}_h \tag{27}$$

is computable from the knowledge of the degrees of freedom. Therefore, there is no need to introduce any approximation in the structure of the terms $(\mathbf{div}\, \boldsymbol{\tau}, \mathbf{u})$ and $(\mathbf{div}\, \boldsymbol{\sigma}, \mathbf{v})$ in problem (2). Instead, the term

$$a_E(\boldsymbol{\sigma}_h, \boldsymbol{\tau}_h) = \int_E \mathbb{D}\boldsymbol{\sigma}_h : \boldsymbol{\tau}_h \tag{28}$$

is not computable for a general couple $(\boldsymbol{\sigma}_h, \boldsymbol{\tau}_h) \in \Sigma_h(E) \times \Sigma_h(E)$. As usual in the VEM approach (see [1], for instance), we then need to introduce a suitable approximation $a_E^h(\cdot,\cdot)$ of $a_E(\cdot,\cdot)$. To this end, we first define the projection operator

$$\begin{cases} \Pi_E \,:\, \Sigma_h(E) \to \mathcal{P}_0(E)_s^{2\times 2} \\ \boldsymbol{\tau}_h \mapsto \Pi_E \boldsymbol{\tau}_h \\ a_E(\Pi_E \boldsymbol{\tau}_h, \boldsymbol{\pi}_0) = a_E(\boldsymbol{\tau}_h, \boldsymbol{\pi}_0) \qquad \forall \boldsymbol{\pi}_0 \in \mathcal{P}_0(E)_s^{2\times 2}. \end{cases} \tag{29}$$

Above and in the sequel, given a domain $\omega$ and an integer $k \geq 0$, the space $\mathcal{P}_k(\omega)$ denotes the polynomials up to degree $k$, defined on $\omega$. Furthermore, given a functional space $X$, $X_s^{2\times 2}$ denotes the $2 \times 2$ symmetric tensors whose components belong to $X$. Therefore, the operator in (29) is a projection onto the piecewise constant symmetric tensors. It is easily seen that $\Pi_E$ is computable, as we suppose that $\mathbb{D}_{|e}$ is constant (cf. Remark 2).

We then set

$$\begin{aligned} a_E^h(\boldsymbol{\sigma}_h, \boldsymbol{\tau}_h) &= a_E(\Pi_E \boldsymbol{\sigma}_h, \Pi_E \boldsymbol{\tau}_h) + s_E\left((Id - \Pi_E)\boldsymbol{\sigma}_h, (Id - \Pi_E)\boldsymbol{\tau}_h\right) \\ &= \int_E \mathbb{D}(\Pi_E \boldsymbol{\sigma}_h) : (\Pi_E \boldsymbol{\tau}_h) + s_E\left((Id - \Pi_E)\boldsymbol{\sigma}_h, (Id - \Pi_E)\boldsymbol{\tau}_h\right), \end{aligned} \tag{30}$$

where $s_E(\cdot,\cdot)$ is a suitable stabilization term. We propose the following choice:

$$s_E(\boldsymbol{\sigma}_h, \boldsymbol{\tau}_h) := \kappa_E\, h_E \int_{\partial E} \boldsymbol{\sigma}_h \mathbf{n} \cdot \boldsymbol{\tau}_h \mathbf{n}, \tag{31}$$

where $\kappa_E$ is a positive constant to be chosen. For instance, in the numerical examples of Section 4, $\kappa_E$ is set equal to $\frac{1}{2}\mathrm{tr}(\mathbb{D}_{|e})$; however, any norm of $\mathbb{D}_{|e}$ can be used. A possible variant of (31) is provided by

$$s_E(\boldsymbol{\sigma}_h, \boldsymbol{\tau}_h) := \kappa_E \sum_{e \in \partial E} h_e \int_e \boldsymbol{\sigma}_h \mathbf{n} \cdot \boldsymbol{\tau}_h \mathbf{n}. \tag{32}$$

### 3.3. The local loading terms

We need to consider the term, see (2):

$$(\mathbf{f}, \mathbf{v}_h) = \int_\Omega \mathbf{f} \cdot \mathbf{v}_h = \sum_{E \in \mathcal{T}_h} \int_E \mathbf{f} \cdot \mathbf{v}_h. \tag{33}$$

We remark that, since $\mathbf{v}_h \in RM(E)$, computing (33) is possible once a suitable quadrature rule is available for polygonal domains. For such an issue, see for instance [11,37,38].

### 3.4. The discrete scheme

We are now ready to introduce the discrete scheme. We introduce a global approximation space for the stress field, by glueing the local approximation spaces, see (21):

$$\Sigma_h = \left\{ \boldsymbol{\tau}_h \in H(\mathbf{div}\,; \Omega) \,:\, \boldsymbol{\tau}_{h|E} \in \Sigma_h(E) \quad \forall E \in \mathcal{T}_h \right\}. \tag{34}$$

For the global approximation of the displacement field, we take, see (26):

$$U_h = \left\{ \mathbf{v}_h \in L^2(\Omega)^2 \,:\, \mathbf{v}_{h|E} \in U_h(E) \quad \forall E \in \mathcal{T}_h \right\}. \tag{35}$$

Furthermore, given a local approximation of $a_E(\cdot,\cdot)$, see (30), we set

$$a_h(\boldsymbol{\sigma}_h, \boldsymbol{\tau}_h) := \sum_{E \in \mathcal{T}_h} a_E^h(\boldsymbol{\sigma}_h, \boldsymbol{\tau}_h). \tag{36}$$

The method we consider is then defined by

$$\begin{cases} \text{Find } (\boldsymbol{\sigma}_h, \mathbf{u}_h) \in \Sigma_h \times U_h \text{ such that} \\ a_h(\boldsymbol{\sigma}_h, \boldsymbol{\tau}_h) + (\mathbf{div}\, \boldsymbol{\tau}_h, \mathbf{u}_h) = 0 \quad \forall \boldsymbol{\tau}_h \in \Sigma_h \\ (\mathbf{div}\, \boldsymbol{\sigma}_h, \mathbf{v}_h) = -(\mathbf{f}, \mathbf{v}_h) \quad \forall \mathbf{v}_h \in U_h. \end{cases} \tag{37}$$

Introducing the bilinear form $\mathcal{A}_h : (\Sigma_h \times U_H) \times (\Sigma_h \times U_h) \to \mathbb{R}$ defined by

$$\mathcal{A}_h(\boldsymbol{\sigma}_h, \mathbf{u}_h; \boldsymbol{\tau}_h, \mathbf{v}_h) \coloneqq a_h(\boldsymbol{\sigma}_h, \boldsymbol{\tau}_h) + (\mathbf{div}\, \boldsymbol{\tau}_h, \mathbf{u}_h) + (\mathbf{div}\, \boldsymbol{\sigma}_h, \mathbf{v}_h), \tag{38}$$

problem (37) can be written as

$$\begin{cases} \text{Find } (\boldsymbol{\sigma}_h, \mathbf{u}_h) \in \Sigma_h \times U_h \text{ such that} \\ \mathcal{A}_h(\boldsymbol{\sigma}_h, \mathbf{u}_h; \boldsymbol{\tau}_h, \mathbf{v}_h) = -(\mathbf{f}, \mathbf{v}_h) \quad \forall (\boldsymbol{\tau}_h, \mathbf{v}_h) \in \Sigma_h \times U_h. \end{cases} \tag{39}$$

We will prove in Section 5 that our method is first order convergent with respect to the natural norms, see in particular Theorem 5.8. More precisely, the following error estimate holds true.

$$\|\boldsymbol{\sigma} - \boldsymbol{\sigma}_h\|_\Sigma + \|\mathbf{u} - \mathbf{u}_h\|_U \lesssim C\, h, \tag{40}$$

where $C = C(\Omega, \boldsymbol{\sigma}, \mathbf{u})$ is independent of $h$ but depends on the domain $\Omega$ and on the Sobolev regularity of $\boldsymbol{\sigma}$ and $\mathbf{u}$.

## 4. Numerical results

The present section is devoted to the assessment of the proposed methodology through the study of the method accuracy on a selected number of test problems. Applicability to structural analysis is then demonstrated through a classical benchmark.

### 4.1. Accuracy assessment

We consider two boundary value problems on the unit square domain $\Omega = [0, 1]^2$, with known analytical solution, discussed in [24,25]. The material obeys to a homogeneous isotropic constitutive law, see (6), with material parameters assigned in terms of the Lamé constants, here set as $\lambda = 1$ and $\mu = 1$. Plane strain regime is invoked throughout. The tests are defined by choosing a required solution and deriving the corresponding body load $\mathbf{f}$, as synthetically indicated in the following:

- Test *a*

$$\begin{cases} u_1 = x^3 - 3xy^2 \\ u_2 = y^3 - 3x^2y \\ \mathbf{f} = \mathbf{0} \end{cases} \tag{41}$$

- Test *b*

$$\begin{cases} u_1 = u_2 = \sin(\pi x)\sin(\pi y) \\ f_1 = f_2 = -\pi^2\left[-(3\mu + \lambda)\sin(\pi x)\sin(\pi y) + (\mu + \lambda)\cos(\pi x)\cos(\pi y)\right]. \end{cases} \tag{42}$$

As it can be observed, Test *a* is a problem with Dirichlet non-homogeneous boundary conditions, zero loading and a polynomial solution; whereas Test *b* has homogeneous Dirichlet boundary conditions and trigonometric distributed loads with a trigonometric solution.

In order to test the robustness of the proposed procedure with respect to element topology and mesh distortion, eight different meshes are considered, as can be inspected in Fig. 1. Four are *structured* meshes composed of triangles, quadrilaterals, hexagons and a mix of convex and concave quadrilaterals. In the following, such meshes are denoted by the letter "S". Four *unstructured* meshes are considered as well, comprising triangles, quadrilaterals, random polygons and a mix of convex and concave hexagons; these are denoted by the letter "U". In the numerical campaign the mesh size parameter is chosen to be the average edge length, denoted with $\bar{h}_e$. We remark that, under mesh assumptions (**A1**) and (**A2**) and for a quasi-uniform family of mesh, $\bar{h}_e$ is indeed equivalent to both $h_E$ and $h$. The accuracy and the convergence rate assessment are carried out using the following error norms:

- Discrete error norms for the stress field:

$$E_{\boldsymbol{\sigma}} \coloneqq \left( \sum_{e \in \mathcal{E}_h} \kappa_e\, h_e \int_e |(\boldsymbol{\sigma} - \boldsymbol{\sigma}_h)\mathbf{n}|^2 \right)^{1/2}, \tag{43}$$

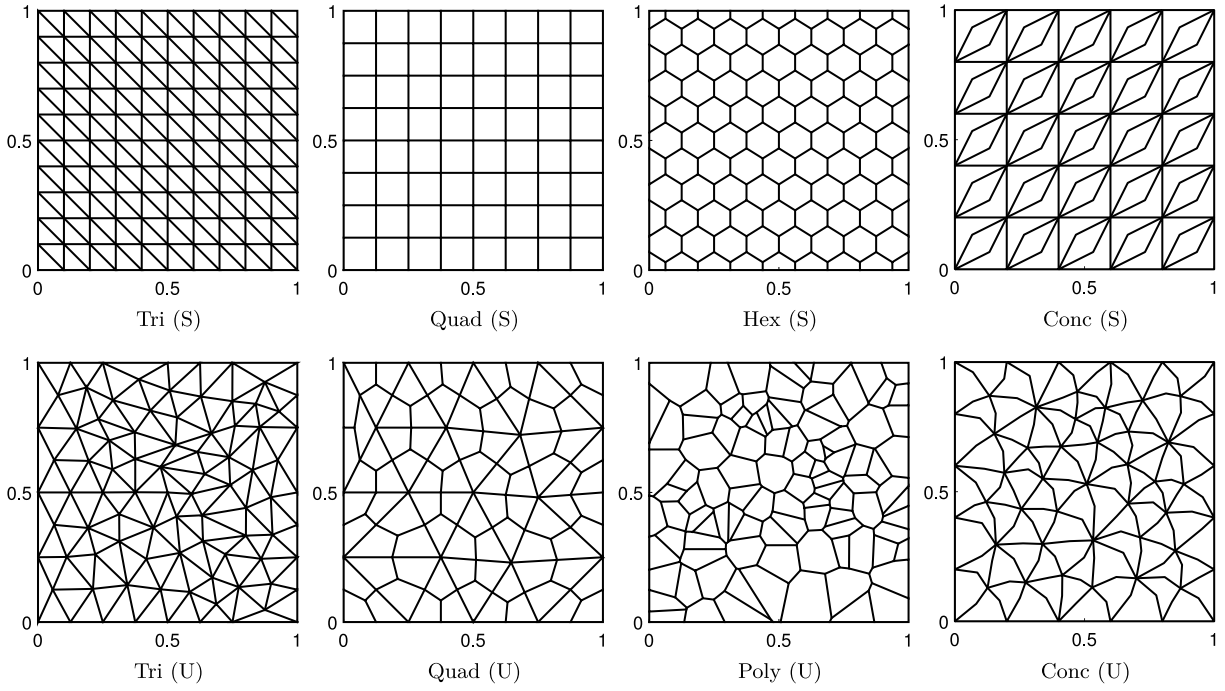


**Fig. 1.** Overview of adopted meshes for convergence assessment numerical tests.

where $\kappa_e = \kappa = \frac{1}{2}\mathrm{tr}(\mathbb{D})$ (the material is here homogeneous). We remark that the quantity above scales like the internal elastic energy, with respect to the size of the domain and of the elastic coefficients.

We make also use of the $L^2$ error on the divergence:

$$E_{\boldsymbol{\sigma},\mathbf{div}} := \left( \sum_{E\in\mathcal{T}_h} \int_E |\mathbf{div}(\boldsymbol{\sigma} - \boldsymbol{\sigma}_h)|^2 \right)^{1/2}. \tag{44}$$

- $L^2$ error norm for the displacement field:

$$E_{\mathbf{u}} := \left( \sum_{E\in\mathcal{T}_h} \int_E |\mathbf{u} - \mathbf{u}_h|^2 \right)^{1/2} = \|\mathbf{u} - \mathbf{u}_h\|_0. \tag{45}$$

Fig. 2 reports the $\bar{h}_e-$convergence of the proposed method for Test $a$. As expected, the asymptotic convergence rate is approximately equal to 1 for all the considered error norms and meshes. It is noted that, in this case, the $E_{\boldsymbol{\sigma},\mathbf{div}}$ plots are not reported because such a quantity is captured up to machine precision for all the considered computational grids.

Fig. 3 reports $\bar{h}_e-$convergence for Test $b$. Asymptotic converge rate is approximately equal to 1 for all investigated mesh types and error measures, including $E_{\boldsymbol{\sigma},\mathbf{div}}$. These results highlight the expected optimal performance of the proposed VEM approach and its robustness with respect to the adopted computational grid.

*4.1.1. Nearly incompressibility regime*

A problem on the unit square domain $\Omega = [0,1]^2$, with known analytical solution, is considered. A nearly incompressible material is chosen by selecting Lamé constants as $\lambda = 10^5$, $\mu = 0.5$. The test is designed by choosing a required solution for the displacement field and deriving the load $\mathbf{f}$ accordingly. The displacement solution is as follows:

$$\begin{cases} u_1 = 0.5(\sin(2\pi x))^2 \sin(2\pi y)\cos(2\pi y) \\ u_2 = -0.5(\sin(2\pi y))^2 \sin(2\pi x)\cos(2\pi x). \end{cases} \tag{46}$$

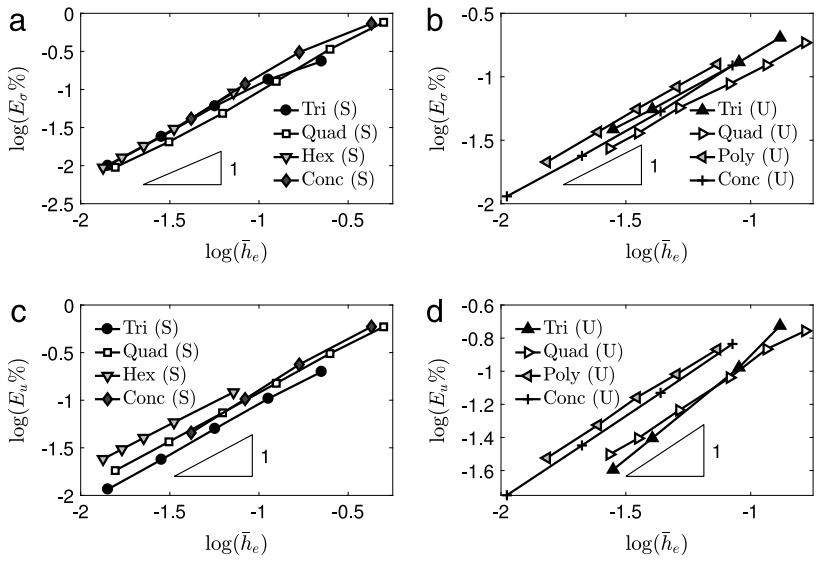


**Fig. 2.** $\bar{h}_e-$convergence results for Test *a* on structured and unstructured meshes: (a) and (b) $E_{\boldsymbol{\sigma}}$ error norm plots, (c) and (d) $E_{\mathbf{u}}$ error norm plots.

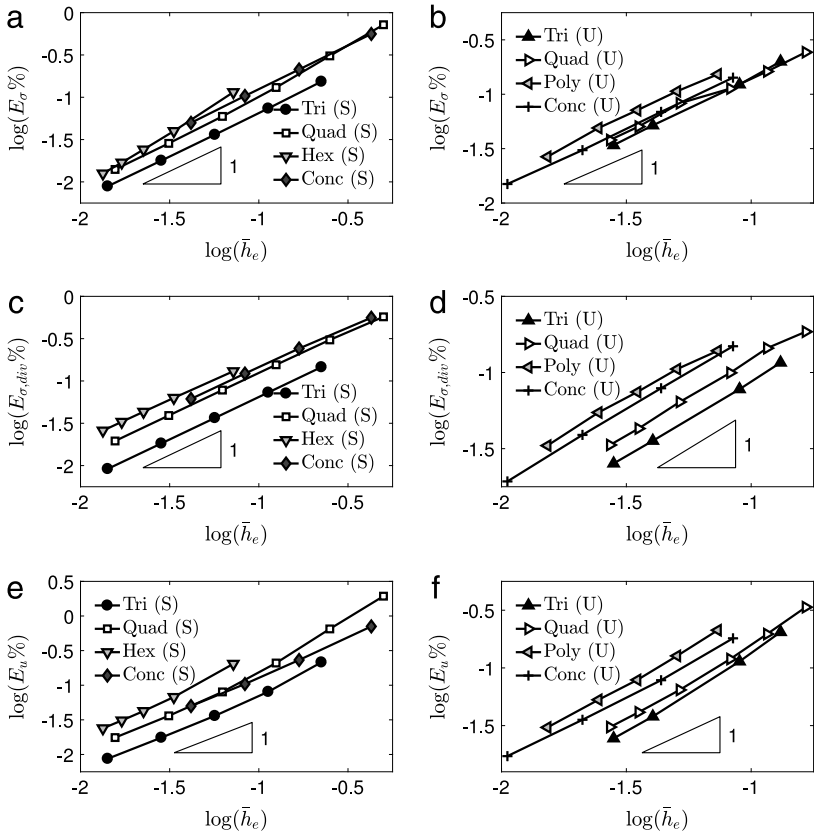


**Fig. 3.** $\bar{h}_e-$convergence results for Test *b* on structured and unstructured meshes: (a) and (b) $E_{\boldsymbol{\sigma}}$ error norm plots, (c) and (d) $E_{\boldsymbol{\sigma},\mathbf{div}}$ error norm plots, (e) and (f) $E_{\mathbf{u}}$ error norm plots.

Fig. 4 reports the results obtained for both structured and unstructured meshes. In can be clearly seen that the proposed method shows the expected asymptotic rate of convergence also in this case.

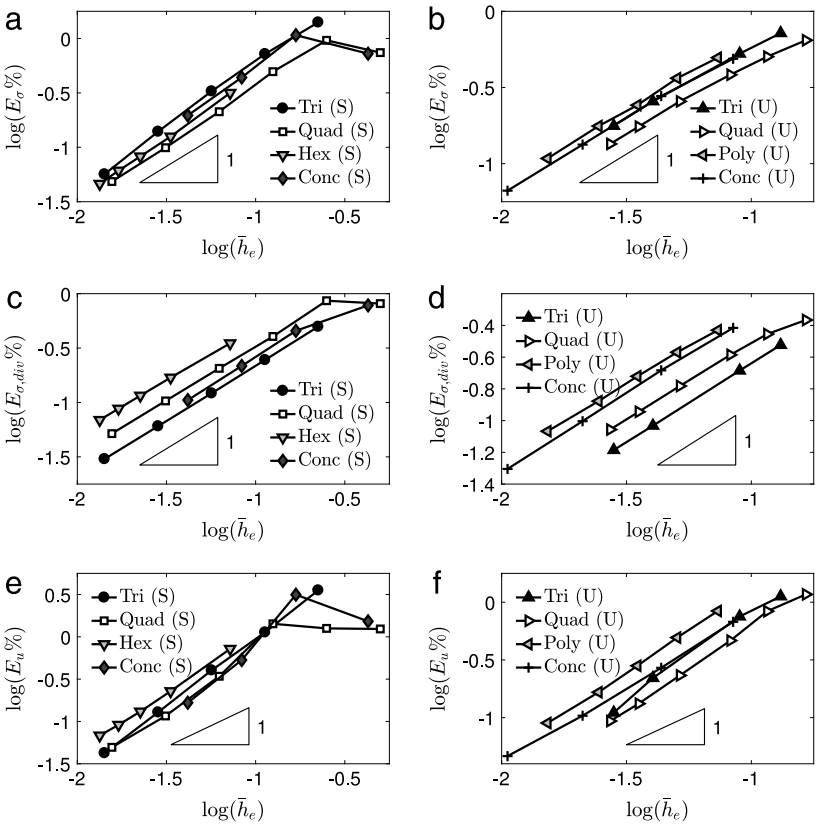


**Fig. 4.** Results for the nearly incompressible test on structured and unstructured meshes: (a) and (b) convergence of $E_{\boldsymbol{\sigma}}$, (c) and (d) convergence of $E_{\boldsymbol{\sigma},\mathbf{div}}$, (e) and (f) convergence for $E_{\mathbf{u}}$.

### *4.2. Structural analysis benchmark: Cook's membrane*

The present section deals with the classical Cook's membrane 2D problem [39]. The geometry of the domain $\Omega$ is presented in Fig. 5 with length data $H_1 = 44$, $H_2 = 16$, $L = 48$. The loading is given by a constant tangential traction $q = 6.25$ on the right edge of the domain. The Young modulus, $E$, is set equal to 70 and two Poisson ratios are considered, one corresponding to $\nu = 1/3$ and one corresponding to a nearly incompressible case characterized by $\nu = 0.499995$.

The problem is solved using three types of meshes: an evenly distributed quadrilateral mesh denoted as Quad, a centroid based Voronoi tessellation, denoted as CVor, and a random based Voronoi tessellation indicated as RVor. An overview of the adopted meshes is reported in Fig. 6.

Convergence results are reported in terms of mesh refinement monitoring $v_A$, the vertical displacement of point A (see Fig. 5), approximated as the vertical displacement at the centroid of the closest polygon. In particular, Fig. 7(a) corresponds to the case in which $\nu = 1/3$ while Fig. 7(b) reports the results obtained for the nearly incompressible case. The reference solution is indicated with a dotted red line corresponding to an overkilling accurate solution obtained with the hybrid-mixed CPE4I element [40]. In accordance with the results of Section 4.1.1, it can be clearly observed that the proposed formulation is robust with respect to the compressibility parameter, as the convergence behaviour of both cases (a) and (b) is almost the same.

Finally, contours representing the von Mises equivalent stress distributions are reported in Fig. 8. We remark that, despite the stress distribution is not known inside the element, its projection $\Pi_E \boldsymbol{\sigma}_h$ onto the constant tensors is explicitably computable (cf. (29)). Thus, we have used this latter quantity to compute the von Mises equivalent stress displayed in Fig. 8. Finally, the results refer to the case $\nu = 1/3$, being the nearly incompressible case extremely similar.

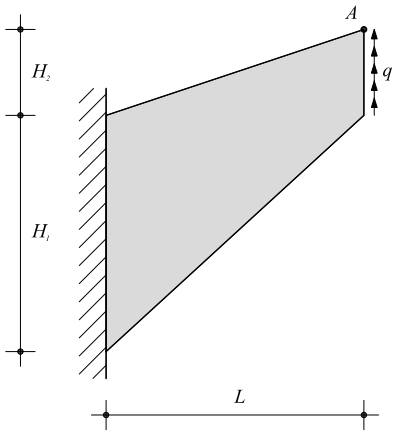


**Fig. 5.** Cook's membrane. Geometry, loading and boundary conditions.

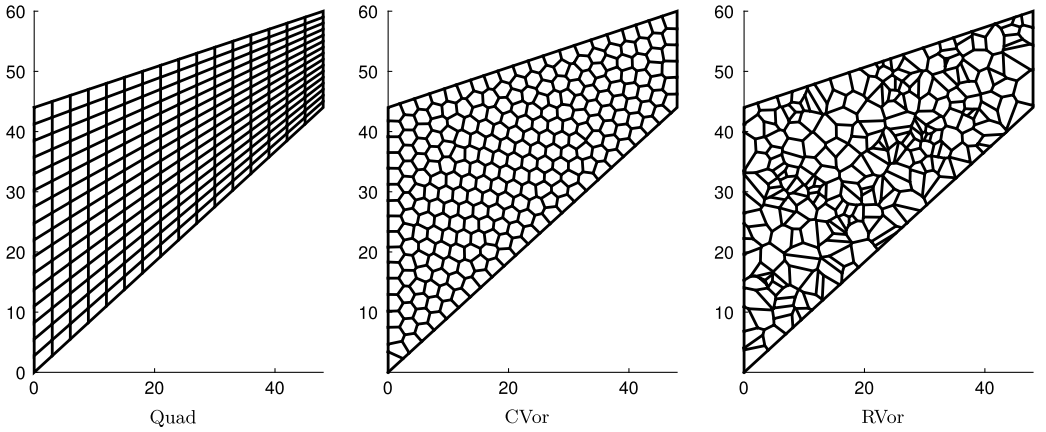


**Fig. 6.** Cook's membrane. Examples of the adopted meshes.

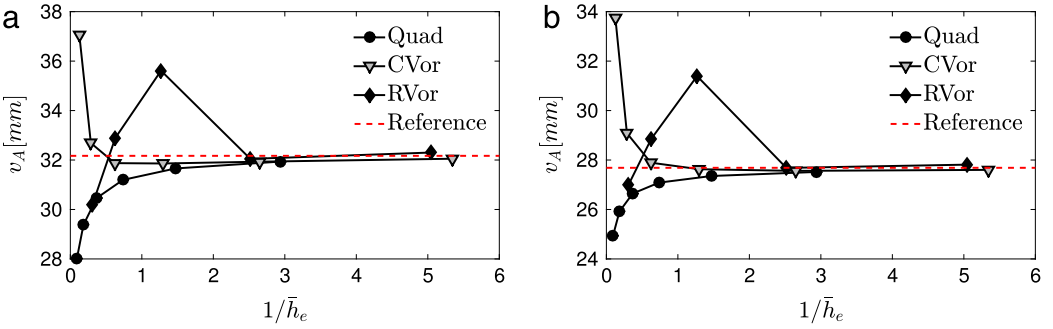


**Fig. 7.** Convergence of the tip vertical displacement $v_A$: (a) $\nu = 1/3$ and (b) $\nu = 0.499995$.

## 5. Stability and convergence analysis

In this section, we provide a rigorous analysis of the proposed VEM method. For all $E \in \mathcal{T}_h$, we first introduce the space:

$$\widetilde{\Sigma}(E) := \left\{ \boldsymbol{\tau} \in H(\mathbf{div}\,; E) \;:\; \exists \mathbf{w} \in H^1(E)^2 \text{ such that } \boldsymbol{\tau} = \mathbb{C}\boldsymbol{\varepsilon}(\mathbf{w}) \right\}. \tag{47}$$

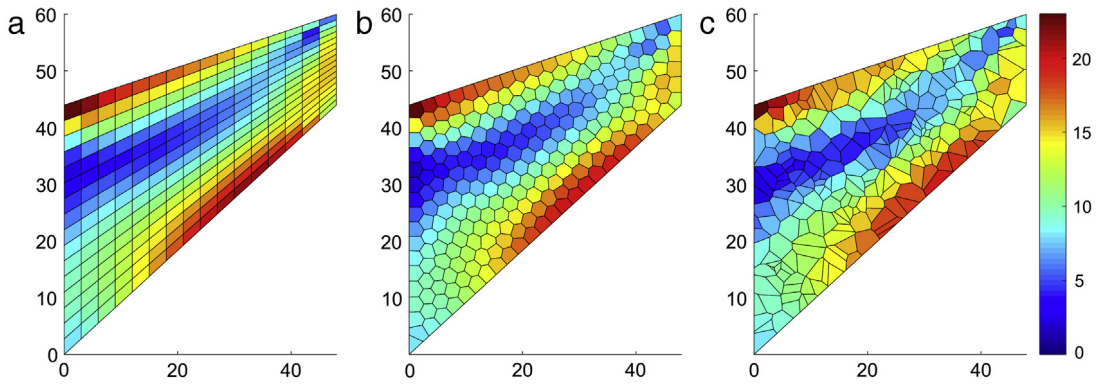


**Fig. 8.** Contours representing the von Mises equivalent stress distributions for $\nu = 1/3$: (a) Quad, (b) CVor, (c) RVor.

The global space $\widetilde{\Sigma}$ is defined as

$$\widetilde{\Sigma} := \left\{ \boldsymbol{\tau} \in H(\mathbf{div}\,; \Omega) \ : \ \exists \mathbf{w} \in H^1(\Omega)^2 \text{ such that } \boldsymbol{\tau} = \mathbb{C}\boldsymbol{\varepsilon}(\mathbf{w}) \right\}. \tag{48}$$

In the sequel, given a measurable subset $\omega \subseteq \Omega$ and $r > 2$, we will use the space

$$W^r(\omega) := \left\{ \boldsymbol{\tau} \ : \boldsymbol{\tau} \in L^r(\omega)^{2\times 2} \ , \ \boldsymbol{\tau} = \boldsymbol{\tau}^T \ , \ \mathbf{div}\,\boldsymbol{\tau} \in L^2(\omega)^2 \right\}, \tag{49}$$

equipped with the obvious norm. Under our assumptions on the mesh, we recall the following version of the Korn's inequality:

$$\inf_{\mathbf{r}\in RM(E)} \left( h_E^{-1} \|\mathbf{v} - \mathbf{r}\|_{0,E} + |\mathbf{v} - \mathbf{r}|_{1,E} \right) \lesssim \|\boldsymbol{\varepsilon}(\mathbf{v})\|_{0,E} \qquad \forall \mathbf{v} \in H^1(E)^2. \tag{50}$$

Given $\mathbf{v} \in H^1(E)^2$, the above inequality can be derived by classical results (see [41], for instance), and by choosing $\mathbf{r}_\mathbf{v} \in RM(E)$ such that $\int_E (\mathbf{v} - \mathbf{r}_\mathbf{v}) = \mathbf{0}$.

We will also use the following result.

**Lemma 5.1.** *Suppose that assumptions* (**A1**) *and* (**A2**) *are fulfilled. Given $E \in \mathcal{T}_h$, let $\mathbf{w} \in H^1(E)^2$ be a solution of the problem:*

$$\begin{cases} -\mathbf{div}(\mathbb{C}\boldsymbol{\varepsilon}(\mathbf{w})) = \mathbf{g} & \text{in } E \\ (\mathbb{C}\boldsymbol{\varepsilon}(\mathbf{w}))\mathbf{n} = \mathbf{h} & \text{on } \partial E, \end{cases} \tag{51}$$

*where $\mathbf{g} \in L^2(E)^2$ and $\mathbf{h} \in L^2(\partial E)^2$ satisfy the compatibility condition*

$$\int_E \mathbf{g} \cdot \mathbf{r} + \int_{\partial E} \mathbf{h} \cdot \mathbf{r} = 0 \qquad \forall \mathbf{r} \in RM(E). \tag{52}$$

*Then it holds:*

$$\|\mathbb{C}\boldsymbol{\varepsilon}(\mathbf{w})\|_{0,E} \lesssim h_E \|\mathbf{g}\|_{0,E} + h_E^{1/2} \|\mathbf{h}\|_{0,\partial E}. \tag{53}$$

**Proof.** For every $\mathbf{r} \in RM(E)$, we have

$$\begin{aligned} \|\mathbb{C}\boldsymbol{\varepsilon}(\mathbf{w})\|_{0,E}^2 &\lesssim \int_E \mathbb{C}\boldsymbol{\varepsilon}(\mathbf{w}) : \boldsymbol{\varepsilon}(\mathbf{w}) \\ &= \int_E \mathbb{C}\boldsymbol{\varepsilon}(\mathbf{w}) : \boldsymbol{\varepsilon}(\mathbf{w} - \mathbf{r}) = \int_E \mathbf{g} \cdot (\mathbf{w} - \mathbf{r}) + \int_{\partial E} \mathbf{h} \cdot (\mathbf{w} - \mathbf{r}), \end{aligned} \tag{54}$$

by which we get

$$\|\mathbb{C}\boldsymbol{\varepsilon}(\mathbf{w})\|_{0,E}^2 \lesssim \|\mathbf{g}\|_{0,E} \, \|\mathbf{w} - \mathbf{r}\|_{0,E} + \|\mathbf{h}\|_{0,\partial E} \, \|\mathbf{w} - \mathbf{r}\|_{0,\partial E}. \tag{55}$$

Under assumptions (**A1**) and (**A2**), the Agmon's inequality then gives

$$\begin{aligned}\|\mathbb{C}\boldsymbol{\varepsilon}(\mathbf{w})\|_{0,E}^2 \lesssim\ & \|\mathbf{g}\|_{0,E}\,\|\mathbf{w}-\mathbf{r}\|_{0,E} \\ & + \|\mathbf{h}\|_{0,\partial E}\left(h_E^{-1/2}\|\mathbf{w}-\mathbf{r}\|_{L^2(E)} + h_E^{1/2}|\mathbf{w}-\mathbf{r}|_{H^1(E)}\right).\end{aligned} \tag{56}$$

Estimate (53) now follows from (50). □

### 5.1. An interpolation operator for stresses

We now introduce the local interpolation operator $\mathcal{I}_E : W^r(E) \to \Sigma_h(E)$, defined as follows. Given $\boldsymbol{\tau} \in W^r(E)$, $\mathcal{I}_E\boldsymbol{\tau} \in \Sigma_h(E)$ is determined by:

$$\int_{\partial E} (\mathcal{I}_E\boldsymbol{\tau})\mathbf{n}\cdot\boldsymbol{\varphi}_* = \int_{\partial E} \boldsymbol{\tau}\mathbf{n}\cdot\boldsymbol{\varphi}_* \qquad \forall \boldsymbol{\varphi}_* \in R_*(\partial E), \tag{57}$$

where (recall that $\mathbf{x}_C$ is the barycentre of $E$):

$$R_*(\partial E) = \left\{\boldsymbol{\varphi}_* \in L^2(\partial E)^2 \,:\, \boldsymbol{\varphi}_{*|e} = \boldsymbol{\gamma}_e + \delta_e(\mathbf{x}-\mathbf{x}_C)^\perp \quad \boldsymbol{\gamma}_e \in \mathbb{R}^2,\ \delta_e \in \mathbb{R},\ \forall e \in \partial E\right\}. \tag{58}$$

If $\boldsymbol{\tau}$ is not sufficiently regular, the integral on the right-hand side of (57) is intended as a duality between $W^{-\frac{1}{r},r}(\partial E)^2$ and $W^{\frac{1}{r},r'}(\partial E)^2$. If $\boldsymbol{\tau}$ is a regular function, the above condition is equivalent to require:

$$\begin{cases} \displaystyle\int_e (\mathcal{I}_E\boldsymbol{\tau})\mathbf{n} = \int_e \boldsymbol{\tau}\mathbf{n} \qquad \forall e \in \partial E; \\ \displaystyle\int_e (\mathcal{I}_E\boldsymbol{\tau})\mathbf{n}\cdot(\mathbf{x}-\mathbf{x}_C)^\perp = \int_e \boldsymbol{\tau}\mathbf{n}\cdot(\mathbf{x}-\mathbf{x}_C)^\perp \qquad \forall e \in \partial E. \end{cases} \tag{59}$$

The following result shows, in particular, that $\mathcal{I}_E\boldsymbol{\tau} \in \Sigma_h(E)$ is well-defined by conditions (57).

**Lemma 5.2.** *Take $\boldsymbol{\tau}_h \in \Sigma_h(E)$. Condition*

$$\int_{\partial E} \boldsymbol{\tau}_h\mathbf{n}\cdot\boldsymbol{\varphi}_* = 0 \qquad \forall \boldsymbol{\varphi}_* \in R_*(\partial E) \tag{60}$$

*implies $\boldsymbol{\tau}_h = \mathbf{0}$.*

**Proof.** First, recall that for $\boldsymbol{\tau}_h \in \Sigma_h(E)$ it holds $(\boldsymbol{\tau}_h\mathbf{n})_{|e} = \mathbf{c}_e + d_e s\,\mathbf{n}$ for each edge $e \in \partial E$, cf. (20) and (21). By (60), choosing $\boldsymbol{\varphi}_*$ such that $\boldsymbol{\varphi}_{*|e} = \boldsymbol{\gamma}_e$ for each $e \in \partial E$, it follows that $(\boldsymbol{\tau}_h\mathbf{n})_{|e} = d_e s\,\mathbf{n}$. Choosing now $\boldsymbol{\varphi}_{*|e} = \delta_e(\mathbf{x}-\mathbf{x}_C)^\perp$, conditions (60) then give

$$d_e \int_e s\,\mathbf{n}\cdot(\mathbf{x}-\mathbf{x}_C)^\perp = 0 \qquad \forall e \in \partial E. \tag{61}$$

A direct computation (for instance by using the Cavalieri–Simpson rule) shows that (61) is equivalent to

$$d_e \frac{|e|}{12}\,\mathbf{n}\cdot(\mathbf{q}_e - \mathbf{p}_e)^\perp = 0 \qquad \forall e \in \partial E. \tag{62}$$

Above, $\mathbf{p}_e$ and $\mathbf{q}_e$ denote the endpoints of $e$. From (62) we infer $d_e = 0$ for each $e \in \partial E$, which concludes the proof. □

The global interpolation operator $\mathcal{I}_h : W^r(\Omega) \to \Sigma_h$ is then defined by simply glueing the local contributions provided by $\mathcal{I}_E$. More precisely, we set $(\mathcal{I}_h\tau)_{|e} := \mathcal{I}_E\boldsymbol{\tau}_{|e}$ for every $E \in \mathcal{T}_h$ and $\boldsymbol{\tau} \in W^r(\Omega)$.

### 5.2. Approximation estimates

**Proposition 5.3.** *Under assumptions* (**A1**) *and* (**A2**)*, for the interpolation operator $\mathcal{I}_E$ defined in* (59)*, the following estimates hold:*

$$\|\boldsymbol{\tau} - \mathcal{I}_E\boldsymbol{\tau}\|_{0,E} \lesssim h_E|\boldsymbol{\tau}|_{1,E} \qquad \forall \boldsymbol{\tau} \in \widetilde{\Sigma}(E) \cap H^1(E)^{2\times 2}. \tag{63}$$

$$\|\mathbf{div}(\boldsymbol{\tau} - \mathcal{I}_E\boldsymbol{\tau})\|_{0,E} \lesssim h_E|\mathbf{div}\,\boldsymbol{\tau}|_{1,E} \ \ \forall \boldsymbol{\tau} \in \widetilde{\Sigma}(E) \cap H^1(E)^{2\times 2} \text{ s.t. } \mathbf{div}\,\boldsymbol{\tau} \in H^1(E)^2. \tag{64}$$

**Proof.** Let $\boldsymbol{\tau} \in \widetilde{\Sigma}(E) \cap H^1(E)^{2\times 2}$, and let $\mathbf{w} \in H^1(E)^2$ be such that $\boldsymbol{\tau} = \mathbb{C}\boldsymbol{\varepsilon}(\mathbf{w})$, see (47). Furthermore, consider $\mathcal{I}_E\boldsymbol{\tau} \in \Sigma_h(E)$ and $\mathbf{w}^* \in H^1(E)^2$ such that $\mathcal{I}_E\boldsymbol{\tau} = \mathbb{C}\boldsymbol{\varepsilon}(\mathbf{w}^*)$, see (21). Hence, setting $\boldsymbol{\delta} := (\mathbf{w} - \mathbf{w}^*) \in H^1(E)^2$, it holds:

$$\boldsymbol{\tau} - \mathcal{I}_E\boldsymbol{\tau} = \mathbb{C}\boldsymbol{\varepsilon}(\boldsymbol{\delta}). \tag{65}$$

Furthermore, using (59), (24) and (25), we infer that $\boldsymbol{\delta} \in H^1(E)^2$ satisfies:

$$\begin{cases} \mathbf{div}(\mathbb{C}\boldsymbol{\varepsilon}(\boldsymbol{\delta})) = \mathbf{div}\,\boldsymbol{\tau} - \dfrac{1}{|E|}\displaystyle\sum_{e\in\partial E}\int_e \boldsymbol{\tau}\mathbf{n} - \frac{(\mathbf{x}-\mathbf{x}_C)^\perp}{\int_E |\mathbf{x}-\mathbf{x}_C|^2}\sum_{e\in\partial E}\int_e \boldsymbol{\tau}\mathbf{n}\cdot(\mathbf{x}-\mathbf{x}_C)^\perp & \text{in } E \\ (\mathbb{C}\boldsymbol{\varepsilon}(\boldsymbol{\delta}))\mathbf{n} = \displaystyle\sum_{e\in\partial E}\left(\boldsymbol{\tau}\mathbf{n} - \frac{1}{|e|}\int_e \boldsymbol{\tau}\mathbf{n}\right)\chi_e & \text{on } \partial E, \end{cases} \tag{66}$$

where $\chi_e$ denotes the characteristic function of the edge $e$. Applying Lemma 5.1 with:

$$\begin{cases} \mathbf{g} := \dfrac{1}{|E|}\displaystyle\sum_{e\in\partial E}\int_e \boldsymbol{\tau}\mathbf{n} + \frac{(\mathbf{x}-\mathbf{x}_C)^\perp}{\int_E |\mathbf{x}-\mathbf{x}_C|^2}\sum_{e\in\partial E}\int_e \boldsymbol{\tau}\mathbf{n}\cdot(\mathbf{x}-\mathbf{x}_C)^\perp - \mathbf{div}\,\boldsymbol{\tau} \\ \mathbf{h} := \displaystyle\sum_{e\in\partial E}\left(\boldsymbol{\tau}\mathbf{n} - \frac{1}{|e|}\int_e \boldsymbol{\tau}\mathbf{n}\right)\chi_e, \end{cases} \tag{67}$$

we get

$$\|\boldsymbol{\tau} - \mathcal{I}_E\boldsymbol{\tau}\|_{0,E} = \|\mathbb{C}\boldsymbol{\varepsilon}(\boldsymbol{\delta})\|_{0,E} \lesssim h_E\|\mathbf{g}\|_{0,E} + h_E^{1/2}\|\mathbf{h}\|_{0,\partial E}. \tag{68}$$

We now estimate $\mathbf{g}$ and $\mathbf{h}$. We denote respectively with $\Pi_{0,E}$, $\Pi_{RM,E}$ and $\Pi_{0,\partial E}$ the $L^2$-projection operators onto the constant functions on $E$, onto the space $RM(E)$ (see (19)), and onto the piecewise constant functions on $\partial E$ (with respect to the edge subdivision of $\partial E$).

The divergence theorem and a direct computation show that:

$$\frac{1}{|E|}\sum_{e\in\partial E}\int_e \boldsymbol{\tau}\mathbf{n} + \frac{(\mathbf{x}-\mathbf{x}_C)^\perp}{\int_E |\mathbf{x}-\mathbf{x}_C|^2}\sum_{e\in\partial E}\int_e \boldsymbol{\tau}\mathbf{n}\cdot(\mathbf{x}-\mathbf{x}_C)^\perp = \Pi_{RM,E}\mathbf{div}\,\boldsymbol{\tau}. \tag{69}$$

Therefore, from the first equation of (67), we have

$$\mathbf{g} = \Pi_{RM,E}\mathbf{div}\,\boldsymbol{\tau} - \mathbf{div}\,\boldsymbol{\tau}. \tag{70}$$

Noting that $\mathcal{P}_0(E)^2 \subset RM(E)$, from the properties of the $L^2$ projection operator, we then get

$$\|\mathbf{g}\|_{0,E} = \|\Pi_{RM,E}\mathbf{div}\,\boldsymbol{\tau} - \mathbf{div}\,\boldsymbol{\tau}\|_{0,E} \le \|\Pi_{0,E}\mathbf{div}\,\boldsymbol{\tau} - \mathbf{div}\,\boldsymbol{\tau}\|_{0,E} \lesssim \|\mathbf{div}\,\boldsymbol{\tau}\|_{0,E} \tag{71}$$

and

$$\|\mathbf{g}\|_{0,E} = \|\Pi_{RM,E}\mathbf{div}\,\boldsymbol{\tau} - \mathbf{div}\,\boldsymbol{\tau}\|_{0,E} \le \|\Pi_{0,E}\mathbf{div}\,\boldsymbol{\tau} - \mathbf{div}\,\boldsymbol{\tau}\|_{0,E} \lesssim h_E|\mathbf{div}\,\boldsymbol{\tau}|_{1,E}. \tag{72}$$

For the second equation of (67), we remark that:

$$\mathbf{h} = \sum_{e\in\partial E}\left(\boldsymbol{\tau}\mathbf{n} - \frac{1}{|e|}\int_e \boldsymbol{\tau}\mathbf{n}\right)\chi_e = \sum_{e\in\partial E}\left(\boldsymbol{\tau} - \frac{1}{|e|}\int_e \boldsymbol{\tau}\right)\mathbf{n}\chi_e = \left(\boldsymbol{\tau} - \Pi_{0,\partial E}\boldsymbol{\tau}\right)\mathbf{n}. \tag{73}$$

Hence, using a standard approximation estimate and a trace inequality, we get

$$\begin{aligned} \|\mathbf{h}\|_{0,\partial E} = \|(\boldsymbol{\tau} - \Pi_{0,\partial E}\boldsymbol{\tau})\mathbf{n}\|_{0,\partial E} &\le \|\boldsymbol{\tau} - \Pi_{0,\partial E}\boldsymbol{\tau}\|_{0,\partial E} \lesssim h_E^{1/2}|\boldsymbol{\tau}|_{1/2,\partial E} \\ &\lesssim h_E^{1/2}|\boldsymbol{\tau}|_{1,E}. \end{aligned} \tag{74}$$

Taking into account (71) and (74), from (68) we obtain estimate (63).

We now notice that from (65)–(67), we have:

$$\mathbf{div}(\boldsymbol{\tau} - \mathcal{I}_E\boldsymbol{\tau}) = -\mathbf{g}. \tag{75}$$

Then, using (72), we immediately get (64). □

### 5.3. Proving the ellipticity-on-the-kernel condition

We first notice that by (29)–(31), using the techniques of [1,42], one has:

$$\|\boldsymbol{\tau}_h\|_{0,E}^2 \lesssim a_E^h(\boldsymbol{\tau}_h, \boldsymbol{\tau}_h) \lesssim \|\boldsymbol{\tau}_h\|_{0,E}^2 \qquad \forall \boldsymbol{\tau}_h \in \Sigma_h(E). \tag{76}$$

We also notice that (see (34), (21) and (35), (26)):

$$\mathbf{div}(\Sigma_h) \subseteq U_h. \tag{77}$$

As a consequence, introducing the discrete kernel $K_h \subseteq \Sigma_h$:

$$K_h = \{\boldsymbol{\tau}_h \in \Sigma_h \,:\, (\mathbf{div}\,\boldsymbol{\tau}_h, \mathbf{v}_h) = 0 \quad \forall \mathbf{v}_h \in U_h\}, \tag{78}$$

we infer that $\boldsymbol{\tau}_h \in K_h$ implies $\mathbf{div}\,\boldsymbol{\tau}_h = \mathbf{0}$. Hence, it holds:

$$\|\boldsymbol{\tau}_h\|_\Sigma = \|\boldsymbol{\tau}_h\|_0 \qquad \forall \boldsymbol{\tau}_h \in K_h. \tag{79}$$

We are now ready to prove the following *ellipticity-on-the-kernel* condition.

**Proposition 5.4.** *For the method described in* Section 3*, there exists a constant* $\alpha > 0$ *such that*

$$a_h(\boldsymbol{\tau}_h, \boldsymbol{\tau}_h) \geq \alpha \|\boldsymbol{\tau}_h\|_\Sigma^2 \qquad \forall \boldsymbol{\tau}_h \in K_h. \tag{80}$$

**Proof.** By recalling (36), from (76) we get the existence of $\alpha > 0$ such that

$$a_h(\boldsymbol{\tau}_h, \boldsymbol{\tau}_h) \geq \alpha \|\boldsymbol{\tau}_h\|_0^2 \qquad \forall \boldsymbol{\tau}_h \in \Sigma_h. \tag{81}$$

Estimate (80) now follows by recalling (79). □

**Remark 5.** Notice that for our method it holds $K_h \subset K$, where $K$ is defined by (7). Considering an isotropic material, see (6), from Remark 1 we infer that the coercivity constant $\alpha$ can be chosen independent of $\lambda$. Therefore, our numerical method does not suffer from volumetric locking (see [43], for instance) and can be used also for nearly incompressible materials. This feature is confirmed by the numerical tests presented in Section 4.

### 5.4. Proving the inf–sup condition

We start by stating the following proposition, which can be derived by regularity results for the elasticity problem on Lipschitz domains (see [44], for example).

**Proposition 5.5.** *Given the polygonal domain* $\Omega$*, there exist* $s > 2$ *and* $\beta^* > 0$ *such that*

$$\sup_{\boldsymbol{\tau} \in W^s(\Omega)} \frac{(\mathbf{div}\,\boldsymbol{\tau}, \mathbf{v})}{\|\boldsymbol{\tau}\|_{W^s(\Omega)}} \geq \beta^* \|\mathbf{v}\|_{0,\Omega} \qquad \forall\, \mathbf{v} \in L^2(\Omega)^2, \tag{82}$$

*where* $W^s(\Omega)$ *is the Banach space defined by* (49).

We are now ready to prove the discrete *inf–sup* condition for our choice of the approximation spaces.

**Proposition 5.6.** *Suppose that assumptions* (**A1**) *and* (**A2**) *are fulfilled. There exists* $\beta > 0$ *such that*

$$\sup_{\boldsymbol{\tau}_h \in \Sigma_h} \frac{(\mathbf{div}\,\boldsymbol{\tau}_h, \mathbf{v}_h)}{\|\boldsymbol{\tau}_h\|_\Sigma} \geq \beta \|\mathbf{v}_h\|_{0,\Omega} \qquad \forall\, \mathbf{v}_h \in U_h. \tag{83}$$

**Proof.** We will apply Fortin's criterion (see [32]), using the operator $\mathcal{I}_h : W^s(\Omega) \to \Sigma_h$, see (59) for the definition of the local contributions. More precisely, we will show that it holds:

$$\begin{cases} \displaystyle\int_\Omega \mathbf{div}(\mathcal{I}_h\boldsymbol{\tau}) \cdot \mathbf{v}_h = \int_\Omega \mathbf{div}\,\boldsymbol{\tau} \cdot \mathbf{v}_h \qquad \forall \mathbf{v}_h \in U_h\,,\ \forall \boldsymbol{\tau} \in W^s(\Omega), \\ \|\mathcal{I}_h\boldsymbol{\tau}\|_\Sigma \lesssim \|\boldsymbol{\tau}\|_{W^s(\Omega)} \qquad \forall \boldsymbol{\tau} \in W^s(\Omega). \end{cases} \tag{84}$$

Together with (82), conditions (84) imply (83), see [32].

To prove the first condition in (84), recalling that $\mathbf{v}_{h|E} \in RM(E)$, it is sufficient to show that:

$$\int_E \mathbf{div}(\mathcal{I}_E\boldsymbol{\tau}) \cdot \mathbf{r} = \int_E \mathbf{div}\,\boldsymbol{\tau} \cdot \mathbf{r} \qquad \forall \mathbf{r} \in RM(E),\ \forall E \in \mathcal{T}_h. \tag{85}$$

The above equation directly follows from the divergence theorem and definition (57).

We now prove the continuity estimate (i.e. the second equation in (84)). We will exploit again Lemma 5.1. More precisely, we take $\mathbf{w}^* \in H^1(E)^2$ such that $\mathcal{I}_E\boldsymbol{\tau} = \mathbb{C}\boldsymbol{\varepsilon}(\mathbf{w}^*)$. It follows that $\mathbf{w}^*$ solves, cf. (69):

$$\begin{cases} \mathbf{div}(\mathbb{C}\boldsymbol{\varepsilon}(\mathbf{w}^*)) = \Pi_{RM,E}\mathbf{div}\,\boldsymbol{\tau} \\ (\mathbb{C}\boldsymbol{\varepsilon}(\mathbf{w}^*))\mathbf{n} = \displaystyle\sum_{e\in\partial E} \mathbf{c}_e\chi_e \qquad \text{on } \partial E, \end{cases} \tag{86}$$

where the $\mathbf{c}_e$'s are given by the dualities for the couple $\langle W^{-\frac{1}{s},s}(\partial E),\, W^{\frac{1}{s},s'}(\partial E)\rangle$:

$$\mathbf{c}_e := \frac{1}{|e|}\left(\langle\boldsymbol{\tau}\mathbf{n},\, \chi_e\mathbf{t}\rangle\mathbf{t} + \langle\boldsymbol{\tau}\mathbf{n},\, \chi_e\mathbf{n}\rangle\mathbf{n}\right). \tag{87}$$

From (86) we obviously deduce

$$\|\mathbf{div}(\mathcal{I}_E\boldsymbol{\tau})\|_{0,E} = \|\mathbf{div}(\mathbb{C}\boldsymbol{\varepsilon}(\mathbf{w}^*))\|_{0,E} = \|\Pi_{RM,E}\mathbf{div}\,\boldsymbol{\tau}\|_{0,E} \le \|\mathbf{div}\,\boldsymbol{\tau}\|_{0,E}. \tag{88}$$

We now apply Lemma 5.1 with:

$$\mathbf{g} := -\Pi_{RM,E}\mathbf{div}\,\boldsymbol{\tau}\,, \quad \mathbf{h} := \sum_{e\in\partial E} \mathbf{c}_e\chi_e, \tag{89}$$

and estimate $\|\mathbf{h}\|_{0,\partial E}$. We start by noting that:

$$\|\mathbf{h}\|_{0,\partial E} = \left(\sum_{e\in\partial E} |\mathbf{c}_e|^2|e|\right)^{1/2} \lesssim h_E^{1/2}\left(\sum_{e\in\partial E} |\mathbf{c}_e|^2\right)^{1/2}. \tag{90}$$

A duality estimate and a trace bound show that

$$\langle\boldsymbol{\tau}\mathbf{n},\, \chi_e\mathbf{t}\rangle \lesssim \|\boldsymbol{\tau}\mathbf{n}\|_{W^{-\frac{1}{s},s}(\partial E)}\|\chi_e\mathbf{t}\|_{W^{\frac{1}{s},s'}(\partial E)} \lesssim \|\boldsymbol{\tau}\mathbf{n}\|_{W^{-\frac{1}{s},s}(\partial E)} \lesssim \|\boldsymbol{\tau}\|_{W^s(E)}. \tag{91}$$

Similarly, it holds:

$$\langle\boldsymbol{\tau}\mathbf{n},\, \chi_e\mathbf{n}\rangle \lesssim \|\boldsymbol{\tau}\|_{W^s(E)}. \tag{92}$$

From (87), (91) and (92) we get

$$|\mathbf{c}_e| \lesssim h_E^{-1}\|\boldsymbol{\tau}\|_{W^s(E)}, \tag{93}$$

by which we deduce, see (90):

$$\|\mathbf{h}\|_{0,\partial E} \lesssim h_E^{-1/2}\|\boldsymbol{\tau}\|_{W^s(E)}. \tag{94}$$

Lemma 5.1 thus gives

$$\|\mathcal{I}_E\boldsymbol{\tau}\|_{0,E} = \|\mathbb{C}\boldsymbol{\varepsilon}(\mathbf{w}^*)\|_{0,E} \lesssim \|\boldsymbol{\tau}\|_{W^s(E)}. \tag{95}$$

The continuity estimate in (84) now follows by collecting all the local estimates (95). □

### 5.5. Error estimates

We denote with $\mathcal{P}_0(\mathcal{T}_h)$ the space of piecewise constant functions with respect to the given mesh $\mathcal{T}_h$. We can prove the proposition:

**Proposition 5.7.** *Suppose that assumptions* **(A1)** *and* **(A2)** *are fulfilled. For every* $(\boldsymbol{\sigma}_I, \mathbf{u}_I) \in \Sigma_h \times U_h$ *and every* $\boldsymbol{\sigma}_\pi \in \mathcal{P}_0(\mathcal{T}_h)^{2\times 2}_s$, *the following error equation holds:*

$$\|\boldsymbol{\sigma} - \boldsymbol{\sigma}_h\|_\Sigma + \|\mathbf{u} - \mathbf{u}_h\|_U \lesssim \|\boldsymbol{\sigma} - \boldsymbol{\sigma}_I\|_\Sigma + \|\mathbf{u} - \mathbf{u}_I\|_U + +h\,\|\mathbf{div}\,\boldsymbol{\sigma}_I\|_{0,\Omega} + \|\boldsymbol{\sigma} - \boldsymbol{\sigma}_\pi\|_{0,\Omega}. \tag{96}$$

**Proof.** Given $(\boldsymbol{\sigma}_I, \mathbf{u}_I) \in \Sigma_h \times U_h$, we form $(\boldsymbol{\sigma}_h - \boldsymbol{\sigma}_I, \mathbf{u}_h - \mathbf{u}_I) \in \Sigma_h \times U_h$. Then, using the *ellipticity-on-the-kernel* condition of Proposition 5.4 and the *inf–sup* condition of Proposition 5.6, there exists $(\boldsymbol{\tau}_h, \mathbf{v}_h) \in \Sigma_h \times U_h$ such that (see [32] and [33], for instance):

$$\|\boldsymbol{\tau}_h\|_\Sigma + \|\mathbf{v}_h\|_U \lesssim 1 \tag{97}$$

and

$$\|\boldsymbol{\sigma}_h - \boldsymbol{\sigma}_I\|_\Sigma + \|\mathbf{u}_h - \mathbf{u}_I\|_U \lesssim \mathcal{A}_h(\boldsymbol{\sigma}_h - \boldsymbol{\sigma}_I, \mathbf{u}_h - \mathbf{u}_I; \boldsymbol{\tau}_h, \mathbf{v}_h). \tag{98}$$

We have

$$\begin{aligned}
\mathcal{A}_h(\boldsymbol{\sigma}_h - \boldsymbol{\sigma}_I, \mathbf{u}_h - \mathbf{u}_I; \boldsymbol{\tau}_h, \mathbf{v}_h) &= \mathcal{A}_h(\boldsymbol{\sigma}_h, \mathbf{u}_h; \boldsymbol{\tau}_h, \mathbf{v}_h) - \mathcal{A}_h(\boldsymbol{\sigma}_I, \mathbf{u}_I; \boldsymbol{\tau}_h, \mathbf{v}_h) \\
&= -(\mathbf{f}, \mathbf{v}_h) - \mathcal{A}_h(\boldsymbol{\sigma}_I, \mathbf{u}_I; \boldsymbol{\tau}_h, \mathbf{v}_h) \\
&= \mathcal{A}(\boldsymbol{\sigma}, \mathbf{u}; \boldsymbol{\tau}_h, \mathbf{v}_h) - \mathcal{A}_h(\boldsymbol{\sigma}_I, \mathbf{u}_I; \boldsymbol{\tau}_h, \mathbf{v}_h) \\
&= [a(\boldsymbol{\sigma}, \boldsymbol{\tau}_h) - a_h(\boldsymbol{\sigma}_I, \boldsymbol{\tau}_h)] + (\mathbf{div}\,\boldsymbol{\tau}_h, \mathbf{u} - \mathbf{u}_I) + (\mathbf{div}(\boldsymbol{\sigma} - \boldsymbol{\sigma}_I), \mathbf{v}_h) \\
&= T_1 + T_2 + T_3.
\end{aligned} \tag{99}$$

Concerning $T_1$, it holds:

$$\begin{aligned}
T_1 &= \sum_{E\in\mathcal{T}_h} \left[a_E(\boldsymbol{\sigma}, \boldsymbol{\tau}_h) - a_E^h(\boldsymbol{\sigma}_I, \boldsymbol{\tau}_h)\right] \\
&= \sum_{E\in\mathcal{T}_h} \Big[a_E(\boldsymbol{\sigma}, \boldsymbol{\tau}_h) - a_E(\Pi_E\boldsymbol{\sigma}_I, \Pi_E\boldsymbol{\tau}_h) \\
&\quad - \kappa_E\, h_E \int_{\partial E} [(Id - \Pi_E)\boldsymbol{\sigma}_I\mathbf{n}] \cdot [(Id - \Pi_E)\boldsymbol{\tau}_h\mathbf{n}]\Big] \quad . \\
&= \sum_{E\in\mathcal{T}_h} \Big[a_E(\boldsymbol{\sigma} - \boldsymbol{\sigma}_\pi, \boldsymbol{\tau}_h) - a_E(\Pi_E(\boldsymbol{\sigma}_I - \boldsymbol{\sigma}_\pi), \Pi_E\boldsymbol{\tau}_h) \\
&\quad - \kappa_E\, h_E \int_{\partial E} [(Id - \Pi_E)\boldsymbol{\sigma}_I\mathbf{n}] \cdot [(Id - \Pi_E)\boldsymbol{\tau}_h\mathbf{n}]\Big].
\end{aligned} \tag{100}$$

We have, using the continuity of $a_E(\cdot,\cdot)$ and of $\Pi_E$:

$$\begin{aligned}
&\sum_{E\in\mathcal{T}_h} \left[a_E(\boldsymbol{\sigma} - \boldsymbol{\sigma}_\pi, \boldsymbol{\tau}_h) - a_E(\Pi_E(\boldsymbol{\sigma}_I - \boldsymbol{\sigma}_\pi), \Pi_E\boldsymbol{\tau}_h)\right] \\
&\lesssim \left(\|\boldsymbol{\sigma} - \boldsymbol{\sigma}_\pi\|_{0,\Omega} + \|\boldsymbol{\sigma}_I - \boldsymbol{\sigma}_\pi\|_{0,\Omega}\right) \|\boldsymbol{\tau}_h\|_{0,\Omega} \\
&\lesssim \left(\|\boldsymbol{\sigma} - \boldsymbol{\sigma}_\pi\|_{0,\Omega} + \|\boldsymbol{\sigma}_I - \boldsymbol{\sigma}\|_{0,\Omega} + \|\boldsymbol{\sigma} - \boldsymbol{\sigma}_\pi\|_{0,\Omega}\right) \|\boldsymbol{\tau}_h\|_{0,\Omega} \\
&\lesssim \left(\|\boldsymbol{\sigma} - \boldsymbol{\sigma}_\pi\|_{0,\Omega} + \|\boldsymbol{\sigma} - \boldsymbol{\sigma}_I\|_{0,\Omega}\right) \|\boldsymbol{\tau}_h\|_\Sigma.
\end{aligned} \tag{101}$$

Furthermore, it holds:

$$\begin{aligned}
&\sum_{E\in\mathcal{T}_h} \kappa_E\, h_E \int_{\partial E} \left[[(Id - \Pi_E)\boldsymbol{\sigma}_I\mathbf{n}] \cdot [(Id - \Pi_E)\boldsymbol{\tau}_h\mathbf{n}]\right] \\
&\lesssim \sum_{E\in\mathcal{T}_h} h_E^{1/2} \|(Id - \Pi_E)\boldsymbol{\sigma}_I\mathbf{n}\|_{0,\partial E} h_E^{1/2} \|(Id - \Pi_E)\boldsymbol{\tau}_h\mathbf{n}\|_{0,\partial E}.
\end{aligned} \tag{102}$$

Under assumptions (**A1**) and (**A2**), we notice that, given $\boldsymbol{\tau}_h \in \Sigma_h(E)$, we have the 1D inverse estimate on $\partial E$:

$$h_E^{1/2} \|\boldsymbol{\tau}_h\mathbf{n}\|_{0,\partial E} \lesssim \|\boldsymbol{\tau}_h\mathbf{n}\|_{-1/2,\partial E} \qquad \forall \boldsymbol{\tau}_h \in \Sigma_h(E). \tag{103}$$

Using the techniques developed in [45], we deduce the scaled trace estimate:

$$\|\boldsymbol{\tau}_h\mathbf{n}\|_{-1/2,\partial E} \lesssim \|\boldsymbol{\tau}_h\|_{0,E} + h_E \|\mathbf{div}\,\boldsymbol{\tau}_h\|_{0,E} \qquad \forall \boldsymbol{\tau}_h \in \Sigma_h(E). \tag{104}$$

Hence, we get:

$$h_E^{1/2} \|\boldsymbol{\tau}_h\mathbf{n}\|_{0,\partial E} \lesssim \|\boldsymbol{\tau}_h\|_{0,E} + h_E \|\mathbf{div}\,\boldsymbol{\tau}_h\|_{0,E} \qquad \forall \boldsymbol{\tau}_h \in \Sigma_h(E). \tag{105}$$

From (102) and (105) we then deduce

$$\begin{aligned}\sum_{E\in\mathcal{T}_h} & \kappa_E\, h_E \int_{\partial E} \left[(Id-\Pi_E)\boldsymbol{\sigma}_I\mathbf{n}\right]\cdot\left[(Id-\Pi_E)\boldsymbol{\tau}_h\mathbf{n}\right] \\ & \lesssim \left(\sum_{E\in\mathcal{T}_h}\left(\|(Id-\Pi_E)\boldsymbol{\sigma}_I\|_{0,E}^2 + h_E^2\|\mathbf{div}\,\boldsymbol{\sigma}_I\|_{0,E}^2\right)\right)^{1/2} \|\boldsymbol{\tau}_h\|_{\Sigma}.\end{aligned} \tag{106}$$

Since it holds, using also the $L^2$ continuity of $\Pi_E$:

$$\begin{aligned}\|(Id-\Pi_E)\boldsymbol{\sigma}_I\|_{0,E}^2 &= \|(\boldsymbol{\sigma}_I-\boldsymbol{\sigma}_\pi)+\Pi_E(\boldsymbol{\sigma}_\pi-\boldsymbol{\sigma}_I)\|_{0,E}^2 \\ &\lesssim \|\boldsymbol{\sigma}_I-\boldsymbol{\sigma}_\pi\|_{0,E}^2 \lesssim \|\boldsymbol{\sigma}_I-\boldsymbol{\sigma}\|_{0,E}^2 + \|\boldsymbol{\sigma}-\boldsymbol{\sigma}_\pi\|_{0,E}^2.\end{aligned} \tag{107}$$

Therefore, we get:

$$\begin{aligned}\sum_{E\in\mathcal{T}_h} & \kappa_E\, h_E \int_{\partial E} \left[(Id-\Pi_E)\boldsymbol{\sigma}_I\mathbf{n}\right]\cdot\left[(Id-\Pi_E)\boldsymbol{\tau}_h\mathbf{n}\right] \\ & \lesssim \left(\|\boldsymbol{\sigma}_I-\boldsymbol{\sigma}\|_{0,\Omega} + \|\boldsymbol{\sigma}-\boldsymbol{\sigma}_\pi\|_{0,\Omega} + h\,\|\mathbf{div}\,\boldsymbol{\sigma}_I\|_{0,\Omega}\right)\|\boldsymbol{\tau}_h\|_{\Sigma}.\end{aligned} \tag{108}$$

Combining (100), (101) and (108), we infer

$$T_1 \lesssim \left(\|\boldsymbol{\sigma}-\boldsymbol{\sigma}_I\|_{0,\Omega} + \|(\boldsymbol{\sigma}-\boldsymbol{\sigma}_\pi)\|_{0,\Omega} + h\,\|\mathbf{div}\,\boldsymbol{\sigma}_I\|_{0,\Omega}\right)\|\boldsymbol{\tau}_h\|_{\Sigma}. \tag{109}$$

Regarding $T_2$, $T_3$ and $T_4$, one obviously has:

$$\begin{cases} T_2 \lesssim \|\mathbf{u}-\mathbf{u}_I\|_U\|\boldsymbol{\tau}_h\|_{\Sigma} \\ T_3 \lesssim \|\boldsymbol{\sigma}-\boldsymbol{\sigma}_I\|_{\Sigma}\|\mathbf{v}_h\|_U. \end{cases} \tag{110}$$

From (98), (99), (109) and (110), we get:

$$\begin{aligned}\|\boldsymbol{\sigma}_h-\boldsymbol{\sigma}_I\|_{\Sigma} + \|\mathbf{u}_h-\mathbf{u}_I\|_U \lesssim \Big(&\|\boldsymbol{\sigma}-\boldsymbol{\sigma}_I\|_{\Sigma} + \|(\boldsymbol{\sigma}-\boldsymbol{\sigma}_\pi)\|_{0,\Omega} \\ &+ h\,\|\mathbf{div}\,\boldsymbol{\sigma}_I\|_{0,\Omega} + \|\mathbf{u}-\mathbf{u}_I\|_U\Big)\left(\|\boldsymbol{\tau}_h\|_{\Sigma} + \|\mathbf{v}_h\|_U\right).\end{aligned} \tag{111}$$

Estimate (96) follows from the triangle inequality, estimate (111) and bound (97). □

We are now ready to state and prove our main convergence result.

**Theorem 5.8.** *Let $(\boldsymbol{\sigma},\mathbf{u}) \in \Sigma\times U$ be the solution of Problem (2), and let $(\boldsymbol{\sigma}_h,\mathbf{u}_h)\in\Sigma_h\times U_h$ be the solution of the discrete problem (37). Suppose that assumptions* (**A1**) *and* (**A2**) *are fulfilled. Assuming $\boldsymbol{\sigma}_{|E}\in H^1(E)^{2\times 2}$ and $(\mathbf{div}\,\boldsymbol{\sigma})_{|E}\in H^1(E)^2$, the following estimate holds true:*

$$\|\boldsymbol{\sigma}-\boldsymbol{\sigma}_h\|_{\Sigma} + \|\mathbf{u}-\mathbf{u}_h\|_U \lesssim C(\Omega,\boldsymbol{\sigma},\mathbf{u})\,h, \tag{112}$$

*where $C(\Omega,\boldsymbol{\sigma},\mathbf{u})$ is independent of $h$ but depends on the domain $\Omega$ and on the Sobolev regularity of $\boldsymbol{\sigma}$ and $\mathbf{u}$.*

**Proof.** In Proposition 5.7 let us choose $\boldsymbol{\sigma}_I = \mathcal{I}_h\boldsymbol{\sigma}\in\Sigma_h$ as detailed in Section 5.1, $\mathbf{u}_I = P_0\mathbf{u}\in U_h$ and $\boldsymbol{\sigma}_\pi = P_0\boldsymbol{\sigma}\in\Sigma_h$. Estimate (112) easily follows from Proposition 5.3 and standard approximation results. □

**Remark 6.** An alternative way to develop the stability and error analysis might be the use of suitable mesh-dependent norms, as detailed in [46] for the Poisson problem in mixed form.

## 6. Conclusions

We have proposed, numerically tested and analysed a new Virtual Element Method for the Hellinger–Reissner formulation of two-dimensional elasticity problems. Our scheme is low-order, it has a priori symmetric stresses and it optimally converges. Possible future developments of the present study include the design of higher-order schemes in the framework of the same variational principle. In addition, accurate post-processed displacements might be considered and used for mesh adaptive strategies, based on suitable a posteriori error estimators.

## Acknowledgements

EA gratefully acknowledges the partial financial support of the Italian Ministry of Education, University and Research, MIUR (Program: Consolidate the Foundations 2015; Project: BIOART; Grant number (CUP): E82F16000850005).

## References

[1] L. Beirão da Veiga, F. Brezzi, A. Cangiani, G. Manzini, L.D. Marini, A. Russo, Basic principles of virtual element methods, Math. Models Methods Appl. Sci. 23 (1) (2013) 199–214.
[2] F. Brezzi, K. Lipnikov, M. Shashkov, V. Simoncini, A new discretization methodology for diffusion problems on generalized polyhedral meshes, Comput. Methods Appl. Mech. Engrg. 196 (2007) 3682–3692.
[3] L. Beirão da Veiga, K. Lipnikov, G. Manzini, The Mimetic Finite Difference Method for Elliptic Problems, in: Series MS&A, vol. 11, Springer, 2014.
[4] F. Brezzi, A. Buffa, K. Lipnikov, Mimetic finite differences for elliptic problems, M2AN Math. Model. Numer. Anal. 43 (2009) 277–295.
[5] F. Brezzi, K. Lipnikov, M. Shashkov, Convergence of the mimetic finite difference method for diffusion problems on polyhedral meshes, SIAM J. Numer. Anal. 43 (5) (2005) 1872–1896.
[6] L. Beirão da Veiga, K. Lipnikov, G. Manzini, Arbitrary-order nodal mimetic discretizations of elliptic problems on polygonal meshes, SIAM J. Numer. Anal. 49 (5) (2011) 1737–1760.
[7] L. Beirão da Veiga, K. Lipnikov, G. Manzini, The mimetic finite difference method for elliptic problems, in: MS&A. Modeling, Simulation and Applications, vol. 11, Springer, 2014 xvi+392. MR 3135418.
[8] J.E. Bishop, A displacement-based finite element formulation for general polyhedra using harmonic shape functions, Internat. J. Numer. Methods Engrg. 97 (1) (2014) 1–31. MR 3146670.
[9] J. Bonelle, A. Ern, Analysis of compatible discrete operator schemes for elliptic problems on polyhedral meshes, ESAIM Math. Model. Numer. Anal. 48 (2) (2014) 553–581. MR 3177857.
[10] K. Lipnikov, G. Manzini, M. Shashkov, Mimetic finite difference method, J. Comput. Phys. 257 (2014) 1163–1227.
[11] S.E. Mousavi, N. Sukumar, Numerical integration of polynomials and discontinuous functions on irregular convex polygons and polyhedrons, Comput. Mech. 47 (5) (2011) 535–554.
[12] S. Natarajan, S. Bordas, D.R. Mahapatra, Numerical integration over arbitrary polygonal domains based on Schwarz–Christoffel conformal mapping, Internat. J. Numer. Methods Engrg. 80 (1) (2009) 103–134.
[13] S. Rjasanow, S. Weißer, Higher order BEM-based FEM on polygonal meshes, SIAM J. Numer. Anal. 50 (5) (2012) 2357–2378.
[14] C. Talischi, G.H. Paulino, Addressing integration error for polygonal finite elements through polynomial projections: a patch test connection, Math. Models Methods Appl. Sci. 24 (8) (2014) 1701–1727.
[15] N. Sukumar, A. Tabarraei, Conforming polygonal finite elements, Internat. J. Numer. Methods Engrg. 61 (12) (2004) 2045–2066.
[16] C. Talischi, G.H. Paulino, A. Pereira, I.F.M. Menezes, Polygonal finite elements for topology optimization: A unifying paradigm, Internat. J. Numer. Methods Engrg. 82 (6) (2010) 671–698.
[17] M. Vohralik, B.I. Wohlmuth, Mixed finite element methods: implementation with one unknown per element, local flux expressions, positivity, polygonal meshes, and relations to other methods, Math. Models Methods Appl. Sci. 23 (5) (2013) 803–838.
[18] E. Wachspress, Rational bases for convex polyhedra, Comput. Math. Appl. 59 (6) (2010) 1953–1956.
[19] D. Di Pietro, A. Alexandre Ern, A hybrid high-order locking-free method for linear elasticity on general meshes, Comput. Methods Appl. Mech. Engrg. 283 (0) (2015) 1–21.
[20] A. Rand, A. Gillette, C. Bajaj, Interpolation error estimates for mean value coordinates over convex polygons, Adv. Comput. Math. 39 (2) (2013) 327–347.
[21] J. Wang, X. Ye, A weak Galerkin finite element method for second-order elliptic problems, J. Comput. Appl. Math. 241 (2013) 103–115.
[22] A. Cangiani, E.H. Georgoulis, P. Houston, hp-Version discontinuous Galerkin methods on polygonal and polyhedral meshes, Math. Models Methods Appl. Sci. 24 (10) (2014) 2009–2041.
[23] A.L. Gain, C. Talischi, G.H. Paulino, On the virtual element method for three-dimensional linear elasticity problems on arbitrary polyhedral meshes, Comput. Methods Appl. Mech. Engrg. 282 (2014) 132–160. MR 3269894.
[24] L. Beirão da Veiga, C. Lovadina, D. Mora, A virtual element method for elastic and inelastic problems on polytope meshes, Comput. Methods Appl. Mech. Engrg. 295 (2015) 327–346.
[25] E. Artioli, L. Beirão da Veiga, C. Lovadina, E. Sacco, Arbitrary order 2D virtual elements for polygonal meshes: Part I, elastic problem, Comput. Mech. (2017). http://dx.doi.org/10.1007/s00466-017-1404-5.
[26] E. Artioli, L. Beirão Da Veiga, C. Lovadina, E. Sacco, Arbitrary order 2D virtual elements for polygonal meshes: Part II, inelastic problems, Comput. Mech. (2017). http://dx.doi.org/10.1007/s00466-017-1429-9.
[27] P. Wriggers, W.T. Rust, B.D. Reddy, A virtual element method for contact, Comput. Mech. 58 (2016) 1039–1050.
[28] H. Chi, L. Beirão da Veiga, G.H. Paulino, Some basic formulations of the virtual element method (vem) for finite deformations, Comput. Methods Appl. Mech. Engrg. 318 (2017) 148–192.
[29] O. Andersen, H.M. Nilsen, X. Raynaud, On the use of the virtual element method for geomechanics on reservoir grids, online: https://arxiv.org/abs/1606.09508.
[30] L. Beirão da Veiga, F. Brezzi, L.D. Marini, Virtual elements for linear elasticity problems, SIAM J. Numer. Anal. 51 (2013) 794–812.
[31] F. Brezzi, L.D. Marini, Virtual element method for plate bending problems, Comput. Methods Appl. Mech. Engrg. 253 (2012) 455–462.

[32] D. Boffi, F. Brezzi, M. Fortin, Mixed finite element methods and applications, in: Springer Series in Computational Mathematics, vol. 44, Springer, Heidelberg, 2013 xiv+685, MR 3097958.
[33] D. Braess, Finite Elements. Theory, Fast Solvers, and Applications in Elasticity Theory, third ed., Cambridge University Press, 2007.
[34] L. Beirão Da Veiga, C. Lovadina, G. Vacca, Divergence free virtual elements for the Stokes problem on polygonal meshes, ESAIM: M2AN 51 (2017) 509–535.
[35] J.-L. Lions, E. Magenes, Problèmes aux limites non homogènes et applications, Vol. 1, in: Travaux et Recherches Mathématiques, No. 17, Dunod, Paris, 1968.
[36] W. Prager, J.L. Synge, Approximations in elasticity based on the concept of function space, Quart. Appl. Math. 5 (1947) 241–269.
[37] S.E. Mousavi, H. Xiao, N. Sukumar, Generalized Gaussian quadrature rules on arbitrary polygons, Internat. J. Numer. Methods Engrg. 82 (1) (2010) 99–113.
[38] A. Sommariva, M. Vianello, Product Gauss cubature over polygons based on Green's integration formula, BIT Numer. Math. 47 (2) (2007) 441–453.
[39] O.C. Zienckiewicz, R.L. Taylor, The Finite Element Method, Butterworth Heinemann, 2000.
[40] Dassault Systèmes, ABAQUS Documentation, Providence, RI, 2011.
[41] O. Oleinik, V. Kondratiev, On Korn's inequalities, C. R. Math. Acad. Sci. Paris 308 (1989) 483–487.
[42] F. Brezzi, R.S. Falk, L.D. Marini, Basic principles of mixed virtual element methods, ESAIM Math. Model. Numer. Anal. 48 (4) (2014) 1227–1240.
[43] T.J.R. Hughes, The Finite Element Method. Linear Static and Dynamic Finite Element Analysis, second ed., Dover, 2000.
[44] R. Herzog, C. Meyer, G. Wachsmuth, Integrability of displacement and stresses in linear and nonlinear elasticity with mixed boundary conditions, J. Math. Anal. Appl. 382 (2011) 802–813.
[45] L. Beirão da Veiga, C. Lovadina, A. Russo, Stability analysis for the virtual element methods, preprint, submitted for publication, arXiv:1607.05988.
[46] C. Lovadina, R. Stenberg, Energy norm a posteriori error estimates for mixed finite element methods, Math. Comp. 75 (256) (2006) 1659–1674 (electronic). MR 2240629 (2007h:65129).